Universiteit Leiden
The Netherlands

Arabidopsis AGC3 kinases and PIN plasma membrane abundance

Gelderen, K. van

Citation

Gelderen, K. van. (2017, July 6). *Arabidopsis AGC3 kinases and PIN plasma membrane abundance*. Retrieved from https://hdl.handle.net/1887/50504

Version:	Not Applicable (or Unknown)
License:	Licence agreement concerning inclusion of doctoral thesis in the Institutional Repository of the University of Leiden
Downloaded from:	https://hdl.handle.net/1887/50504

Note: To cite this publication please use the final published version (if applicable).

Cover Page

Universiteit Leiden

Leiden University Repository

The handle http://hdl.handle.net/1887/50504 holds various files of this Leiden University dissertation

Author: Gelderen, Kasper van
Title: Arabidopsis AGC3 kinases and PIN plasma membrane abundance
Issue Date: 2017-07-06

Chapter 2

The *Arabidopsis* AGC3-4 kinase acts opposite to PINOID in apical/basal PIN polarity

Kasper van Gelderen[1,3], Carlos Galvan Ampudia[1,4], Michael Karampelias[2], Fang Huang[1,5], Yang Xiong[1,6], Jiri Friml[2,7], Remko Offringa[1,#]

[1] Plant developmental genetics, Institute of Biology, Leiden University, Sylviusweg 72, 2333 BE Leiden, The Netherlands.
[2] Department of Plant Systems Biology, VIB, and Department of Plant Biotechnology and Bioinformatics, Ghent University, 9052 Gent, Belgium
[3] Current affiliation: Plant Ecophysiology, Institute of Environmental Biology, Utrecht University, Padualaan 8, 3584 CH Utrecht, The Netherlands.
[4] Current affiliation: Laboratoire de Reproduction et Développement des Plantes, CNRS, INRA, ENS Lyon, UCBL, Université de Lyon, 69364 Lyon, France.
[5] Current affiliation: The University of Liverpool, Institute of Integrative Biology, Biosciences Building, Crown Street, Liverpool L69 7ZB, UK.
[6] Current affiliation: College of Life Sciences, Peking University, Beijing 100871, China.
[7] Current affiliation: Institute of Science and Technology Austria, 3400 Klosterneuburg, Austria
[#] Author for correspondence: r.offringa@biology.leidenuniv.nl

Abstract

The unequal distribution of the plant hormone auxin by directional cell-to-cell transport is essential for plant development. This polar auxin transport (PAT) is mediated by PIN-FORMED (PIN) auxin efflux carriers that determine the direction of PAT through their asymmetric positioning on the plasma membrane. Phosphorylation of PINs by the Arabidopsis AGC3 protein serine/threonine kinase PINOID (PID) and its closest homologs WAG1 and WAG2 results in PIN localization at the apical (shootward) side of the plasma membrane. Here we revisited the presumed redundancy between the *AGC3* kinase genes, and observed that *WAG2* and the fourth AGC3 kinase gene, *AGC3-4*, could not complement *pid* when fused with the *PID* promoter, most likely because of instability of both proteins in the *PID* expression domain. Surprisingly, unlike the other three kinases, AGC3-4 did not induce the same basal to apical shift in PIN polarity. Loss-of-function *agc3-4* mutants showed minor defects in root growth and gravitropism, but combined *agc3* loss-of-function mutations did not provide evidence for a redundant function with the other AGC3 kinases. *AGC3-4* overexpression resulted in auxin transport related phenotypes, such as dwarf growth, reduced root gravitropism and delayed lateral root emergence, correlating with an increased basal (rootward) PIN polarity. *AGC3-4* expression was predominantly observed in tissues (vasculature, stomatal lineage) where PINs are either basal or apolar. These findings together with the *AGC3-4* overexpression-induced enhanced sensitivity of PIN1 and PIN2 to the ARF-GEF GNOM inhibitor BFA indicate that AGC3-4 promotes GNOM-dependent recycling of PINs back to the plasma membrane and thus acts opposite to its close homologs PID, WAG1 and WAG2.

Introduction

Plant development and growth are for a large part regulated by the unequal distribution of the plant hormone auxin in developing plant tissues, which is established through the polar cell to cell transport of auxin (Habets and Offringa, 2014). The PIN FORMED (PIN) auxin efflux carriers are rate-limiting components in this polar auxin transport that determine the direction of transport through their asymmetric subcellular distribution on the plasma membrane (Petrásek et al., 2006; Wisniewska et al., 2006). The establishment of PIN polarity following their apolar secretion occurs by clathrin-mediated endocytosis, polar exocytosis and immobilization of PINs in plasma membrane microdomains (Kleine-Vehn et al., 2011). Clathrin-mediated endocytosis of PINs from the plasma membrane involves the ADP Ribosylation Factor (ARF) and GTPase SCARFACE (Dhonukshe et al., 2007; Sieburth et al., 2006), while recycling back to the plasma membrane is dependent on the ARF GTP Exchange Factor (GEF) GNOM in the case of basal PIN polarity and by another yet unknown ARF-GEF in the case of shootward polarity (Geldner et al., 2001; Geldner et al., 2003; Kleine-Vehn et al., 2008a; Kleine-Vehn et al., 2009). The fungal toxin Brefeldin A (BFA) blocks GNOM and thus causes a buildup of PINs normally targeted towards basal polarity into BFA-bodies (Geldner et al., 2003). Recently, evidence was provided that GNOM and GNOM-Like 1 mediate secretion of PINs to the basal plasma membrane(Doyle et al., 2015), suggesting that delivery of newly synthesized PINs to the plasma membrane can be polar. Phosphorylation of PINs at conserved serines in the TPRXS motif by the plasma membrane-associated AGC protein serine threonine kinases PID, WAG1 and WAG2 results in GNOM-independent trafficking of PINs to the plasma membrane (Dhonukshe et al., 2010; Friml et al., 2004; Huang et al., 2010; Kleine-Vehn et al., 2009). Phosphorylation by these kinases can switch PIN polarity from basal (rootward) to apical (shootward) in root- and shoot meristem cells (Dhonukshe et al., 2010; Friml et al., 2004; Kleine-Vehn et al., 2009), from inner to outer lateral in hypocotyl endodermis cells (Ding et al., 2011; Friml et al., 2002; Furutani et al., 2014), or from neck to lobe in leaf pavement cells (Li et al., 2011; Xu et al., 2010).

AGC3-4 is a homolog of PID, and together with PID, WAG1 and WAG2 it forms the AGC3 subclade of *Arabidopsis thaliana* AGCVIII kinases (Galván-Ampudia and Offringa, 2007). The PID, WAG1 and WAG2 kinases are important for root and shoot development (Benjamins et al., 2001; Cheng et al., 2008; Dhonukshe et al., 2010; Huang et al., 2010) and tropisms (Ding et al., 2011; Preuten et al., 2013; Santner and Watson, 2006; Zhang et al., 2013). However, a clear role for AGC3-4 was not apparent, since the no-cotyledon phenotype reported for the *pid wag1 wag2 agc3-4* quadruple mutant (Cheng et al., 2008) is already fully penetrant for the *pid wag1 wag2* triple mutant (Dhonukshe et al., 2010). Moreover, the effect of AGC3-4 overexpression on PIN polarity has not yet been tested. The high amino acid identity between the conserved sub-domains of the catalytic kinase domain of PID

and AGC3-4 (Galván-Ampudia and Offringa, 2007) suggests that their functions might be similar. However, an important difference lies in the insertion domain in the activation segment of these kinases that is typical for the plant-specific AGCVIII kinase group. This insertion domain is relatively long in AGC3-4 and more similar to the one found in AGC1 clade kinases, such as D6PK (Rademacher and Offringa, 2012).

Here we analyzed the redundancy among AGC3 kinase in more detail, focusing on the function of AGC3-4 in Arabidopsis development by comparing single and higher order *acg3* loss-off-function mutants or overexpression lines for phenotypes and effects on PIN trafficking. Our findings show that AGC3-4 promotes basal polarity of PIN1 and PIN2 and that it thus acts opposite to the other AGC3 kinases PID, WAG1, and WAG2.

Results

AGC3-4 does not act redundantly with the other AGC3 kinases in Arabidopsis development

Higher order loss-of-function mutants of the AGC3 kinase genes *PID, WAG1* and *WAG2* have progressively severe developmental defects and show altered environmental responses. At the seedling level, *pid wag1 wag2* triple mutants show a fully penetrant no cotyledon phenotype, and develop shorter roots that are defective in geotropism (Cheng et al., 2008; Dhonukshe et al., 2010). We analyzed two *AGC3-4* SAIL-insertion-line alleles, *agc3-4-1* and *agc3-4-2* (Fig. S3). *agc3-4-2* loss-of-function mutant seedlings showed a significant reduction in root length at 11 and 13 days after germination, similar to the *pid* mutant, indicating the involvement of both genes in root growth (Fig. 1A-C,H). For the *pid wag1 wag2* triple mutant, the root length was strongly reduced, as observed previously (Dhonukshe et al., 2010), while the addition of the *agc3-4-2* mutation did not lead to a further reduction in the root length (Fig. 1D-G,H). The *agc3-4-1* loss-of-function mutant showed a delay in root gravitropic growth, and this defect could be complemented by an *AGC3-4::AGC3-4-YFP* construct (Fig. 1I-K). Interestingly, plant lines overexpressing *AGC3-4* (*35S::AGC3-4-YFP*) showed a similar delay in gravitropic root growth as *agc3-4-1* (Fig. 1I,L). During vegetative development, the *agc3-4-2* single mutant was indistinguishable from wild type, whereas the *agc3-4-2 wag1 wag2* triple loss-of-function mutant showed a similar reduction in rosette diameter and leaf area as the *pid* single mutant (Fig. 1M-S). The triple *pid wag1 wag2* mutant was severely affected in both rosette diameter and rosette leaf area (Fig. 1Q-S) and although the *agc3-4 pid wag1 wag2* quadruple mutant was not tested in this experiment, its rosette growth appeared to be reduced in the same order as the triple mutant in other experiments (Fig. 2G,H).

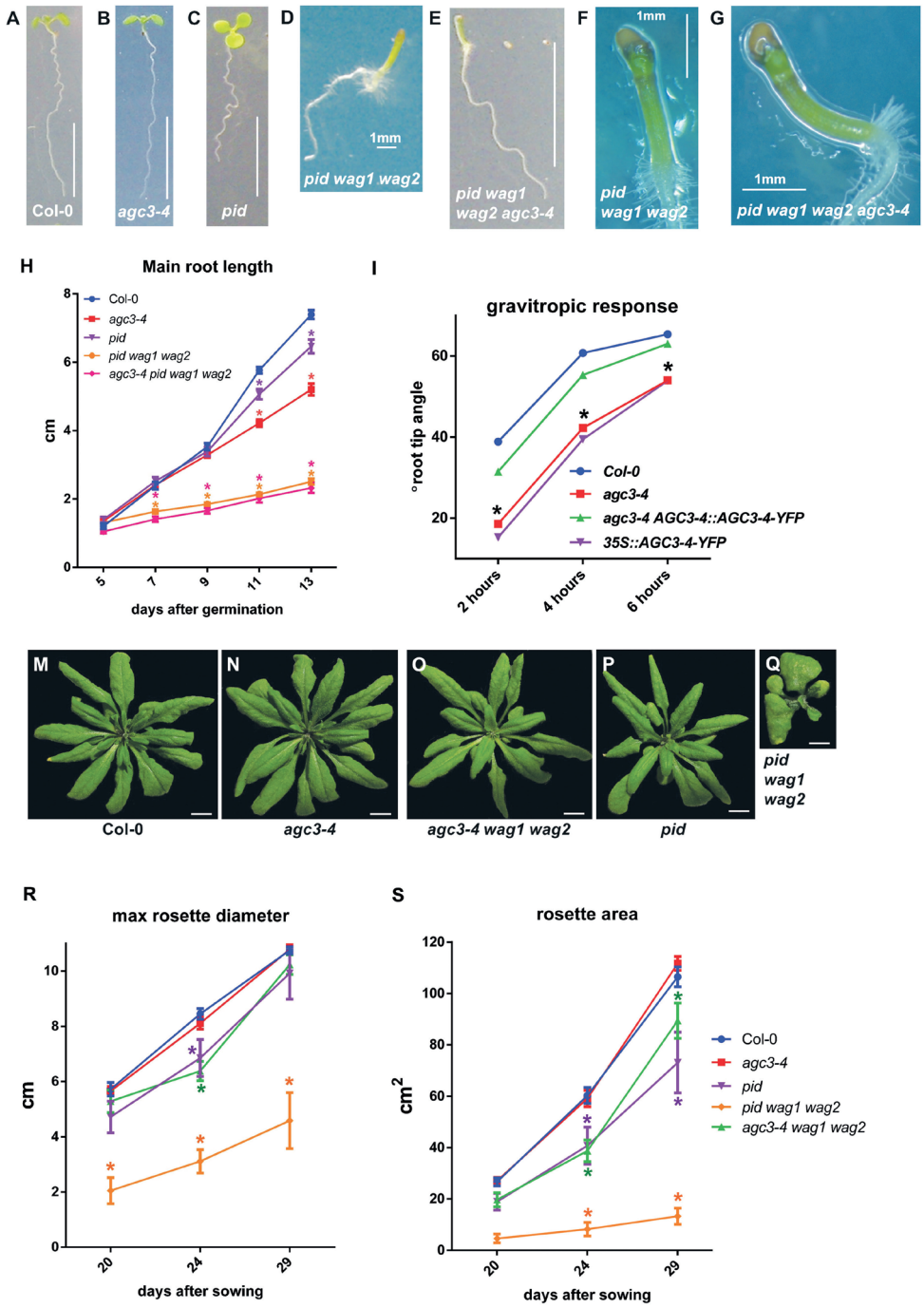

Figure 1: *AGC3-4* acts in root growth, but not in shoot development.
(A-G) Six day old seedlings of Col-0 (A), *agc3-4-2* (B), *pid-14* (C), *pid wag1 wag2* (D, triple mutant) *and pid wag1 wag2 agc3-4-2* (E, quadruple mutant), with F and G zooming in on the shoot of a triple or quadruple mutant seedling. (H) Average main root length analysis of light grown 5 to 13 day old seedlings (n=12). (I-L) Root gravitropic

response of four day old wild-type (Col-0), *agc3-4-1*, *agc3-4-1 AGC3-4::AGC3-4-YFP* and *35S::AGC3-4-YFP* seedlings (n=20-30). The angle between the root axis and growing tip was measured. (M-Q) Rosette phenotype of five weeks old Col-0 (M), *agc3-4-2* (N), *agc3-4-2 wag1 wag2* (O), *pid-14* (P) and *pid-14 wag1 wag2* (Q) plants, and quantification of (R) the maximal rosette diameter and (S) rosette area of these plants (n=8-12). Error bars depict the standard error of the mean, and asterisks in the graphs indicate a significant difference with Col-0 (p<0,05, 2-way ANOVA + tukey post-hoc test). Scale bars indicate 1 mm in F and G or 1cm in all other images.

At the flowering plant stage, *agc3-4-2* mutants were indistinguishable from wild-type plants (Fig. 2A,B), whereas higher order mutants containing the *pid-14* allele and one or both of the *wag* mutations again showed progressively severe developmental defects. Adult *pid wag1* and *pid wag2* plants developed mainly pin-formed inflorescences that, compared to those of the *pid* single mutant, showed strong branching, while the *pid agc3-4-2* double mutant did not show significantly stronger phenotypes (Fig. 2C-F). *pid wag1 wag2* triple mutant plants only produced a limited number of aberrantly curled rosette leaves, and a short pin-formed inflorescences (Fig. 2G). As discussed before, the *agc3-4-2 pid wag1 wag2* quadruple mutant did not show a clearly enhanced rosette phenotype compared to the triple mutant (Fig. 2H).

Our analysis confirms the redundancy between the previously analysed AGC3 kinase genes *PID*, *WAG1* and *WAG2*. For *AGC3-4* however, its loss-of-function did not lead to obvious phenotypes other than a reduction in main root growth for one allele and slower geotropism for the other, and these relatively minor phenotypic effects cannot be explained by the redundant action of the other three AGC3 kinases.

WAG2 and AGC3-4 act differently in the inflorescence due to reduced stability

To confirm that PID, WAG1 and WAG2 act redundantly, and AGC3-4 not, we cloned the *AGC3* kinase cDNAs upstream to the YFP-HA coding region and expressed these translational fusions under the *PID* promoter in the *pid wag1 wag2* mutant background. *PID::PID-YFP* and *PID::WAG1-YFP* constructs complemented the *pid wag1 wag2* triple mutant in about 60% of the transformed lines, whereas none of the *PID::WAG2-YFP* and *PID::AGC3-4-YFP* triple mutant transformants showed a wild-type phenotype, as they still developed pin-formed inflorescences (Fig. 3A-H). Although rescuing the *pid wag1 wag2* phenotype and producing seeds, adult *PID::WAG1-YFP* plants occasionally developed pin-formed inflorescences and *pid-like* flowers (Fig. 3C-E). The *PID::WAG2/AGC3-4-YFP* constructs were not able to fully complement the inflorescence phenotype of *pid wag1 wag2* mutant to yield fertile plants, however they did enhance rosette and inflorescence development (Fig. 2G and Fig. 3F,G). When we checked these transgenic lines for the expression of the kinase-YFP-HA fusion proteins by Western blot analysis, we were able to detect PID and WAG1 in young flower buds, whereas WAG2 and AGC3-4 were undetectable in the pin-formed inflorescence apices (Fig. 3J). This suggests that the lack of rescue by *PID::WAG2* and *PID::AGC3-4* may be attributed to an instability of these kinases in the *PID* expression domain.

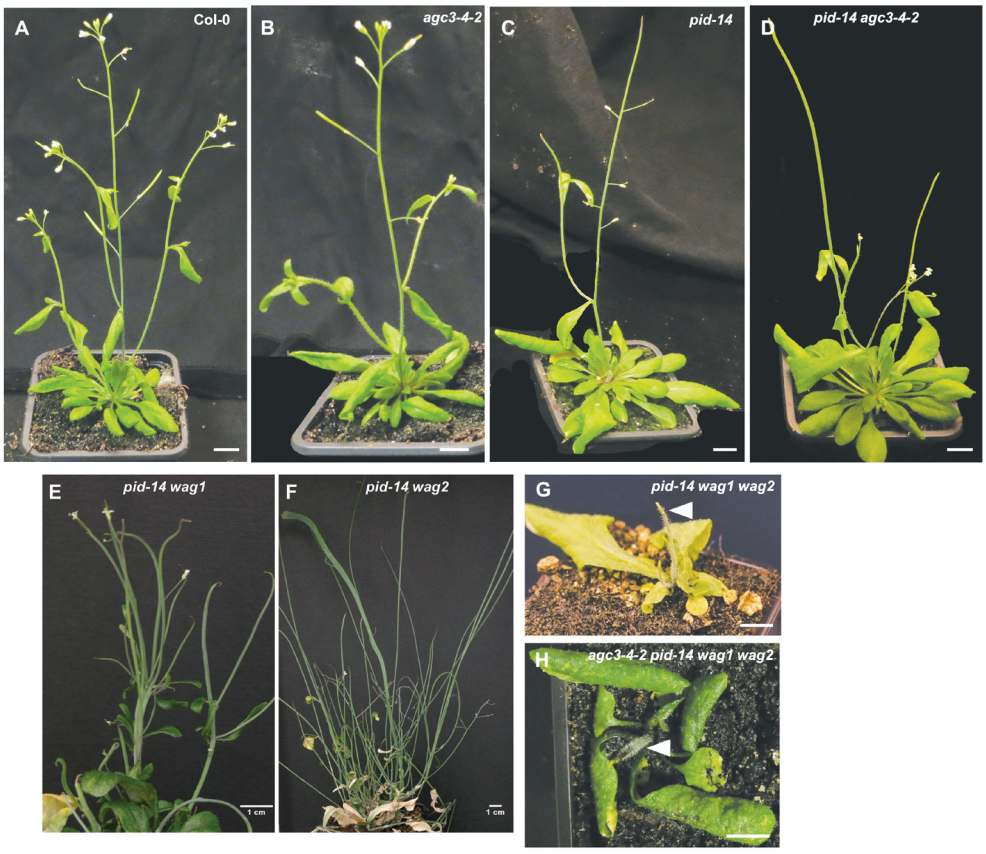

Figure 2: AGC3-4 does not act redundantly with PID in inflorescence development.
(A-H) Flowering plants (6 to 8 weeks old) of Col-0 (A), *agc3-4-2* (B), *pid-14* (C), *pid-14 agc3-4-2* (D), *pid-14 wag1* (E), *pid-14 wag2* (F) and *pid-14 wag1 wag2* triple (G) and *agc3-4-2 pid-14 wag1 wag2* quadruple (H) mutants. The arrowheads indicate the location of the inflorescence. Scale bars depict 1cm.

At the embryo/seedling level, the no-cotyledon phenotype of the *pid wag1 wag2* mutant was fully rescued by the *PID::PID* construct, whereas *PID::WAG1* showed partial complementation. This is in line with our observations on the occasional occurrence of pin-formed inflorescences in flowering *pid wag1 wag2 PID::WAG1-YFP* plant that initially showed wild type development, and might be explained by the previously observed lower kinase activity of WAG1 (Dhonukshe et al., 2010). Surprisingly, around 25% to 30% of the *pid wag1 wag2* seedlings carrying the *PID::PID-YFP* or *PID::WAG1-YFP* construct developed three cotyledons (Fig. 3I). At this point we have no explanation for this observation other than that most likely the *PID* promoter activity does not completely correspond to the spatio-temporal expression of the genomic *PID* gene. The *PID::WAG2-YFP* construct showed no rescue, and the *PID::AGC3-4-YFP* construct only resulted in a slight reduction of the number of no cotyledon seedlings, coinciding with a low percentage of three cotyledon seedlings (Fig. 3I).

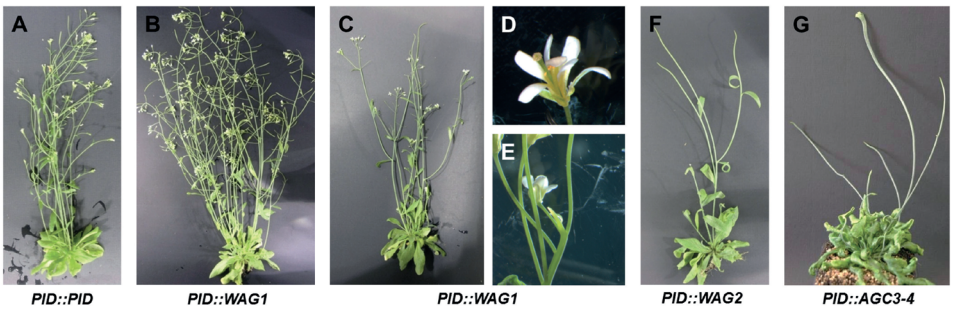

H

Transformants constructed

Construct	*pid,wag1,wag2* homozygous lines	Inflorescence WT	Inflorescence *pid*
PID::PID	17	64%	36%
PID::WAG1	18	61%	39%
PID::WAG2	30	0%	100%
PID::AGC3-4	15	0%	100%

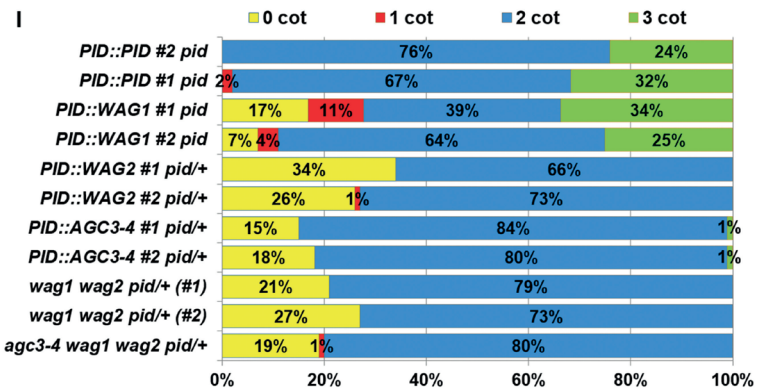

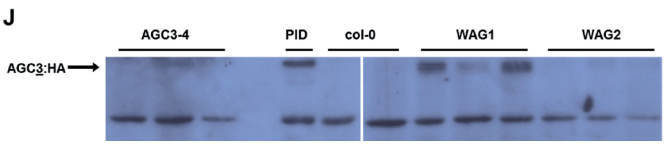

Figure 3: *PID* promoter driven AGC3 kinase expression in the *pid wag wag2* mutant background.
(A-G) Phenotypes of representative flowering plants of *PID::PID-YFP, PID::WAG1-YFP, PID::WAG2-YFP* and *PID::AGC3-4-YFP* lines in the *pid wag1 wag2* triple mutant background. (H) Table depicting the amount of transformants and the percentage of transformants rescuing the pin-formed inflorescence phenotype of the *pid-14 wag1 wag2* mutant. (I) Cotyledon phenotypes of the plant lines shown in A-H and of the *pid-14 wag1 wag2* triple and *agc3-4-2 pid-14 wag1 wag2* quadruple knockout lines (#1 and #2 indicate that individual lines were tested). *PID::WAG2-YFP* and *PID::AGC3-4-YFP* cannot rescue the pin-formed inflorescences of the *pid wag1 wag2* mutant background and, similar to the triple and quadruple mutant lines, progeny were taken from a parental plant that is heterozygous for the *pid-14* allele (noted as *pid/+)* (n is at least 200 seedlings). (J) Western blot analysis showing floral samples of lines used in (I), probed with an anti-HA antibody (arrow indicates expected size of the YFP-HA-tagged kinases). The lower a-specific band was used as a loading control.

The data presented here show that PID and WAG1 act redundantly in the inflorescence. Based on seedling overexpression phenotypes (Cheng et al., 2008; Dhonukshe et al., 2010) and higher order mutant analysis (Fig. 1 and 2) it is clear that WAG2 acts in the same manner on PIN polarity as PID and WAG1. However, the failure of WAG2 to rescue the *pid wag1 wag2* phenotype most likely lies in its instability in the inflorescence. Since we were also unable to detect AGC3-4 in the inflorescence, this experiment did not allow us to draw further conclusions about the role of this PID homolog in plant development.

AGC3-4 shows partial nuclear and plasma membrane localization, like WAG1 and WAG2

When *Arabidopsis* protoplasts were transfected with *35S* promoter driven AGC3 kinase constructs, AGC3-4-YFP showed localization at the plasma membrane, cytosol and the nucleus, where it located to small intense spots (Fig. 4A,B). FM-4-64 staining confirmed plasma membrane and endosomal localization (Fig. 4C-F). In protoplasts, PID was exclusively plasma membrane localized, while WAG1 and WAG2 were also present in the nucleus (Fig. 4G-J), as was reported before (Galván-Ampudia and Offringa, 2007). Interestingly, nuclear WAG1 and WAG2 accumulated in the nucleolus, but not in the small intense spots observed for AGC3-4 (Fig. 4H-J).

Gene-YFP fusions expressed in their corresponding mutant background were used to verify these observations *in planta*. In *agc3-4 AGC3-4::AGC3-4-YFP* seedlings the YFP signal could be observed in lateral root primordia (Fig. 4K), and in the (pro)vascular tissue of roots (Fig. 4L), hypocotyls (Fig. 4M,N), cotyledons and leaves (Fig. 4O,P) and in the cotyledon epidermis where the signal was especially strong in the nuclei of young guard cells and one neighboring young pavement cell (Fig. 4Q). As in protoplasts, AGC3-4-YFP localized both in the nucleus and at the plasma membrane of cells (insets Fig. 4K and L), in contrast to PID-YFP which was found only at the plasma membrane (Fig. 4R,S). The plasma membrane localization of AGC3-4-YFP in the root always appeared somewhat weaker than the nuclear signal and AGC3-4 did not show the apical-basal polarity that was observed for PID in the main root meristem and the lateral root primordia (Fig. 4R,S). WAG1-GFP and WAG2-GFP were previously shown to be localized at the plasma membrane of root epidermis cells (Dhonukshe *et al.*, 2010). In addition, we observed that the WAG1-GFP signal was especially strong in pairs of newly divided cells in the main root meristem and that WAG1-GFP localized in the nucleus in lateral root epidermis cells (Fig. 4U,T).

In summary, all AGC3 kinases localized to the plasma membrane, whereas WAG1, WAG2 and AGC3-4 were also found in the nucleus. Notably, AGC3-4 showed a much weaker PM localization compared to the other AGC3 kinases.

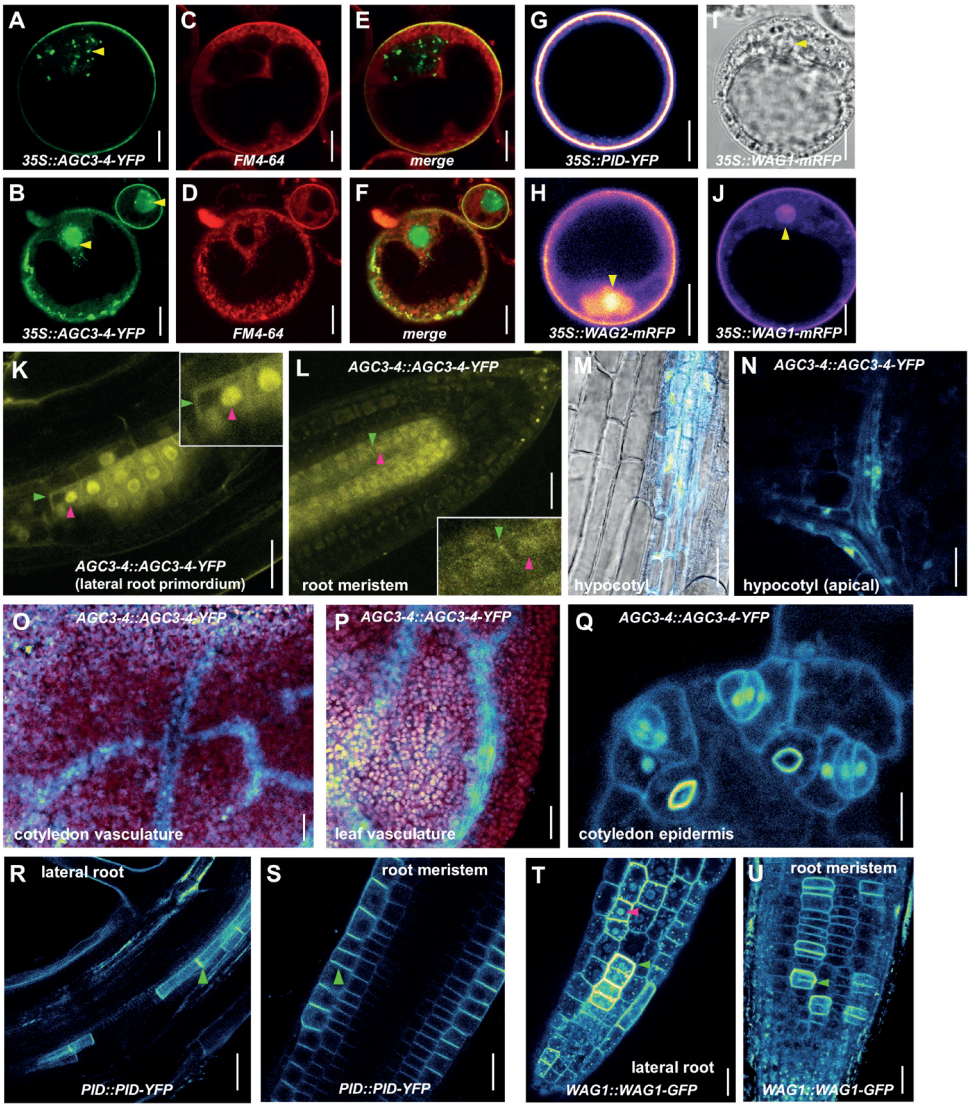

Figure 4: The *AGC3-4* gene encodes a nuclear- and plasma membrane-localized kinase and is expressed in (pro)vascular and leaf epidermis cells.

(A-F) Confocal images of two similar FM4-64-stained *Arabidopsis* protoplasts transfected with *35S::AGC3-4-YFP*, showing the YFP signal (A,B), the FM4-64 signal (C-D) and the merged images (E,F). (G-J) Confocal images of *Arabidopsis* protoplasts transfected with *35S::PID-YFP* (G), *35S::WAG2-mRFP* (H) and *35S::WAG2-mRFP* (J). Yellow arrow heads point to nucleus in (A, B) and to the nucleolus in (H,J). (I) Bright field image of the protoplast in (J), showing the nucleolus. Scale bar in (A-J) indicates 10 µm.

(K-Q) Confocal images of 4 to 6 day old *agc3-4-1 AGC3-4::AGC3-4-YFP* seedlings showing *AGC3-4::AGC3-4-YFP* expression in the lateral root primordium (LRP, K), the root meristem (L), hypocotyl vasculature (M,N), cotyledon vasculature (O), leaf vasculature (P) and in young guard cells and flanking pavement cells in the cotyledon epidermis (Q). The insets in (K and L) show details of the nuclear (pink arrowhead) and plasma membrane (green arrowhead) localization of AGC3-4-YFP. (R-U) Confocal images of 4 to 6 day old seedlings of complementing lines *pid-14 PID::PID-YFP* and *wag1 WAG1::WAG1-GFP*, showing PID-YFP signal at the lateral root primordium (R) or in the root meristem (S), or WAG1-GFP signal at the lateral root meristem (T), or at the main root meristem (U). Pink arrowhead in (T) points to nuclear signal, while green arrowheads (in R,S,U) point out membrane signals. Scale bar in (K-U) indicates 20 µm.

AGC3-4 overexpression leads to dwarfed plants with pleiotropic phenotypes

To gain more information about the function of *AGC3-4, 35S::AGC3-4-CFP* and *-YFP* overexpression constructs were introduced into the Col-0 wild-type and *35S::DII-YFP* (Brunoud et al., 2012) background, and primary transformants with a strong overexpression level were selected using epifluorescence and confocal microscopy (Fig. S1A,B). Seedlings and adult plants of strong *35S::AGC3-4-CFP* lines showed a dwarfed phenotype (Fig. 5A-D), which differs from the agravitropic and root meristem collapse phenotype of *35S::PID/WAG1/WAG2* seedlings (Dhonukshe et al., 2010). The main root and hypocotyl of *35S::AGC3-4-YFP* seedlings were shorter than wild type (Fig. 5E,F), and the

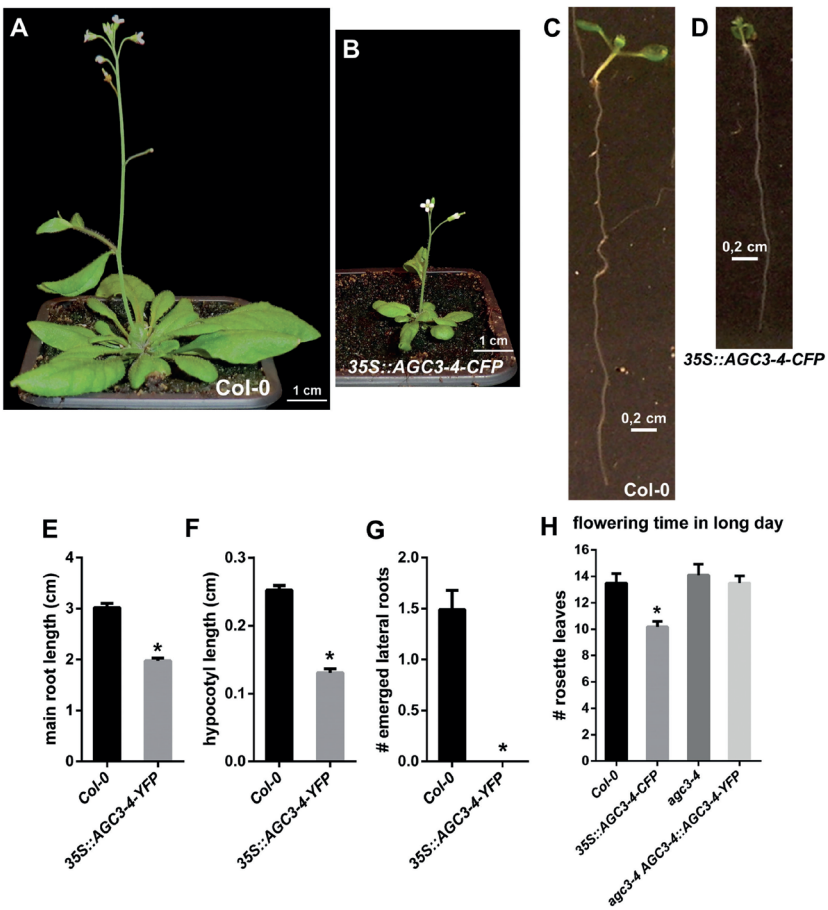

Figure 5: *AGC3-4* overexpression leads to dwarf plants that show delayed lateral root emergence and early flowering.

(A-D) One month old flowering wild-type (Col-0, A) and *35S::AGC3-4-CFP* (B) plants, and one week old wild-type (Col-0, C) and *35S::AGC3-4-CFP* (D) seedlings. (E-G) Main root length, hypocotyl length and lateral root number of 7, 8 and 7 day old wild-type (Col-0) *35S::AGC3-4-YFP* seedlings, respectively. (H) Flowering time for wild-type (Col-0), *35S::AGC3-4-CFP*, *agc3-4-1* and *agc3-4-1 AGC3-4::AGC3-4-YFP* plants grown in long day conditions, as measured by the number of rosette leaves at the time of bolting . Asterisks in the graphs E-H indicate significant differences with wild type (Col-0), (*t*-test, p = < 0,05). Error bars indicate the standard error of the mean.

cotyledons showed epinastic bending (Fig. 5D). Eight days after germination, *35S::AGC3-4-YFP* seedlings did not have emerged lateral roots (Fig. 5G), however earlier stage lateral root primordia were present, and lateral roots emerged approximately 4 days later than in wild-type seedlings (Fig. S1C-F). There was no obvious difference with wild type in the auxin sensitivity of lateral root initiation (Fig. S1G-J). When *35S::AGC3-4-CFP* plants were grown under long day conditions, the flowering time was significantly reduced (Fig. 5H). As stated earlier, *35S::AGC3-4-CFP* seedlings responded slower to a change in the gravity vector, when compared to wild type (Fig. 1I-L). Striking additional phenotypes of adult *35S::AGC3-4-CFP* plants were their reduced rosette size, enhanced apical dominance, and early senescence and occasional stomatal clustering (Fig. S1K-M). The reduced root length, apical dominance, delayed root gravitropy and lower lateral root number of *35S::AGC3-4-CFP* plants hinted at some alteration in auxin distribution. However, these defects were distinctively different from *35S::PID* lines. *35S::PID* plants were slightly smaller than wild type (Fig. S1N), seedlings were completely agravitropic and showed main root meristem collapse (Benjamins et al., 2001; Dhonukshe et al., 2010; Friml et al., 2004). This data strongly suggested that AGC3-4 acted differently on auxin distribution than the other three AGC3 kinases.

AGC3-4 overexpression enhances the relative basal PIN polarity

To confirm a role for AGC3-4 in auxin distribution-related processes, we compared the *35S::DII-YFP* auxin reporter signal (Brunoud et al., 2012) in median confocal sections of wild-type and *35S::AGC3-4-CFP* root tips (Fig. 6A-B). Quantification of the DII-YFP intensity of the individual regions (Fig. S2A) did not show a significant difference between wild-type and *35S::AGC3-4-CFP* roots (Fig. S2B). However, the ratio of the DII-YFP intensity in the outer layers and the stele was significantly lower in *35S::AGC3-4-CFP* roots (Fig. 6E), suggesting a subtle but significant redistribution of auxin from the stele to the outer cell layers of *35S::AGC3-4-CFP* root tips. Quantification of immunolocalized PIN1 detected an increase in the basal/lateral ratio due to a decrease in lateral localization of PIN1 in *35S::AGC3-4-CFP* stele cells (Fig. 6C,D and F,G). Strikingly, this is opposite to the basal to apical shift of PIN1 observed in *PID-*, *WAG1-* or *WAG2* overexpression lines (Dhonukshe et al., 2010; Friml et al., 2004). In *pin2 PIN2::PIN2-YFP* seedlings we observed an increase in the basal/(inner) lateral ratio of PIN2-YFP in the cortex of *35S::AC3-4-CFP* roots compared to wild type (Fig. 6H-J). This effect on PIN2-YFP localization was not observed in *pin2 PIN2::PIN2-YFP S,1,2,3A* seedlings, where PIN2-YFP was predominantly apolar in both wild-type and *35S::AC3-4-CFP* backgrounds (Fig. 6H,K,L).

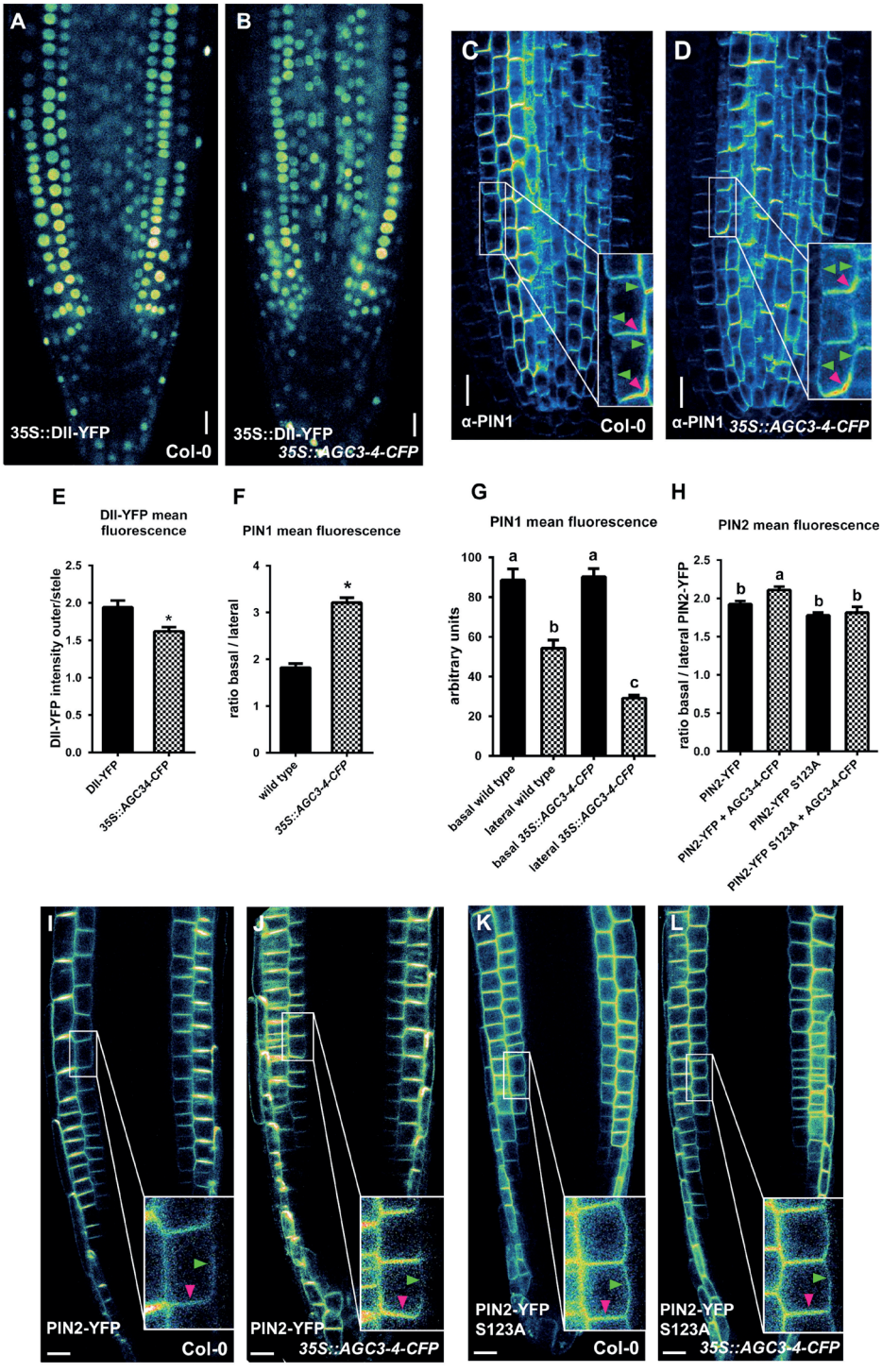

Figure 6: *AGC3-4* overexpression alters auxin distribution and enhances basal polarity of PIN1 and PIN2 in root meristems.

(A,B) NLS-DII-YFP signal in 4 day old wild-type (Col-0, A) or *35S::AGC3-4-CFP* (B) seedlings. (C,D) Immunolocalization of PIN1 in four day old wild-type (Col-0, C) and *35S::AGC3-4-CFP* (D) seedlings (Pink arrowhead = basal, green = lateral). (E) Quantification of NLS-DII-YFP signal in the root meristem: graph showing the ratio between the outer layers and stele (Explanation of the regions selected for quantification in Fig. S2). (F) Quantification of the basal/lateral plasma membrane signal ratio in endodermis and 1st and 2nd layer stele cells and (G) mean fluorescence intensities of the ratios in (F). (H-L) PIN2-YFP signal in root tips of 4 day old *eir1-1 PIN2::PIN2-YFP* (I,J) or *eir1-1 PIN2::PIN2-YFP (S123A)* (K,L) seedlings with or without *35S::AGC3-4:CFP,* with the basal/(inner)lateral plasma membrane signal ratio quantified in (H) (Pink arrowhead = basal, green = inner lateral). All scale bars represent 20 µm. Asterisks in (C,G,H) indicate significant difference with wild-type control (*t*-test , p = < 0,05). Error bars indicate standard error of the mean.

These results indicate that, opposite to the basal to apical shift of PINs induced by the other AGC3 kinases, AGC3-4 increased the relative basal polarity of PIN1 and PIN2, leading to a redistribution of auxin from the stele to the outer cell layers, which resulted in reduced root growth and gravitropism. The opposing effect of AGC3-4 and the other three AGC3 kinases on PIN polarity also explains why AGC3-4 overexpression does not cause root meristem collapse. The enhanced basal localization of PIN2-YFP is dependent on the presence of serine residues in the conserved TPRXS motifs in the PIN hydrophilic loop, suggesting that AGC3-4 exerts its effect by direct PIN2 phosphorylation.

Recycling of PIN-containing vesicles from the early endosome/trans golgi network (EE/TGN) back to the plasma membrane is, in the case of basal PINs, dependent on the ARF-GEF-GNOM (Geldner et al., 2001; Geldner et al., 2003; Kleine-Vehn et al., 2008a; Kleine-Vehn et al., 2009). The fungal toxin BFA blocks GNOM and thus causes a buildup of basally recycled PINs into BFA-bodies. Quantification of BFA bodies following BFA treatment can therefore be used to determine the rate of basal PIN recycling. Treatment of 4 days old wild-type or *35S::AGC3-4-CFP* seedlings with 25µM BFA for 4 and 6 hours resulted in more BFA bodies for both PIN1 and PIN2 in *35S::AGC3-4-CFP* stele and epidermis cells, respectively. Six hours of 25µM BFA treatment resulted in a significantly higher number of PIN1 BFA bodies per *35S::AGC3-4-CFP* root stele cell (Fig. 7A-C). PIN2-containing BFA bodies were also increased in *35S::AGC3-4-CFP* epidermis cells, however in this case the difference was already significant after 4 hours of treatment (Fig. 7D-F). This result indicates that *35S::AGC3-4-CFP* promotes the GNOM-dependent trafficking of PIN1 and PIN2 and thereby increases the relative abundance to the basal plasma membrane.

AGC3-4 phosphorylates the TPRXS motifs in the PIN2 hydrophilic loop *in vitro*

Previously we showed that PID, WAG1 and WAG2 phosphorylate serines in three TPRXS motifs in the PIN hydrophilic loop (PINHL) (Dhonukshe et al., 2010; Huang et al., 2010). In an *in vitro* phosphorylation assay we observed that also AGC3-4 can phosphorylate the wild-type PIN2 HL (Fig. 8A 1st and 2nd lanes). When AGC3-4 was incubated with a PIN2 HL mutant version with the serines in the three TPRXS motifs replaced by Alanines (PIN2 HL S1,2,3,A), no phosphorylation was observed (Fig. 8A last lane), indicating that the kinase

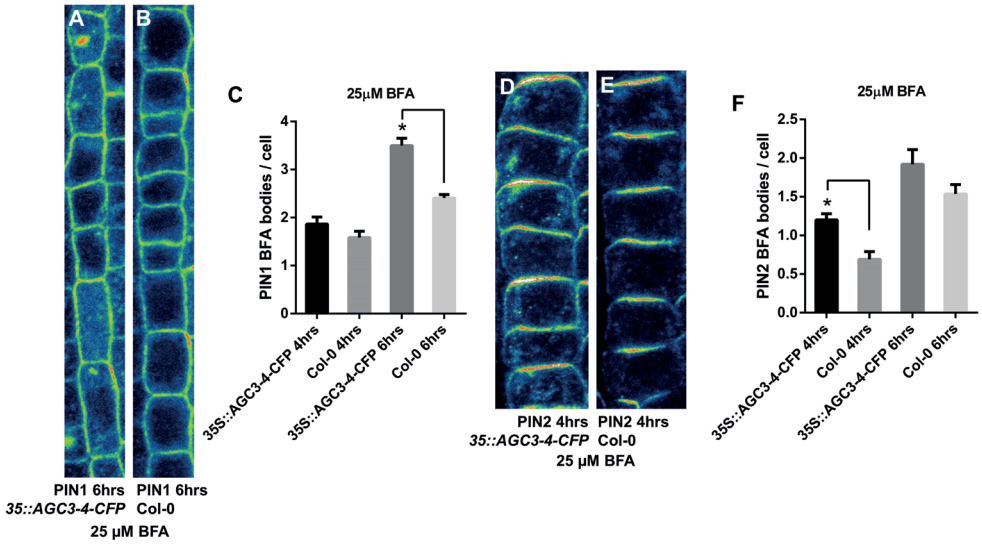

Figure 7: *AGC3-4* overexpression increased PIN1 and PIN2 BFA body formation.
(A-C) PIN1 immunolocalization in the root endodermis of 4 day old *35S::AGC3-4-CFP* (A) or wild-type (Col-0, B) seedlings treated with 25 µM BFA for six hours, and quantification of BFA bodies by manual counting (C). (D-F) PIN2 immunolocalization in root epidermis cells of 4 day old *35S::AGC3-4-CFP* (D) or wild-type (Col-0, E) seedlings treated with 25 µM BFA for four hours, and quantification of BFA bodies (F) Quantification in (C and F) was done on 10 cells per seedling, and 6-10 seedlings per treatment. Asterisks indicate significant differences with wild-type control (p< 0,05, one way ANOVA with post-hoc test). Error bars indicate standard error of the mean.

phosphorylates the same residues as the other three AGC3 kinases. In general, AGC3-4 was less active than PID in phosphorylating the PIN2 HL (Fig. 8B,D) and for both kinases removing S2 had the strongest impact on the phosphorylation efficiency, whereas the S1A mutation had limited effect or even seemed to enhance phosphorylation in the case of AGC3-4. The limited phosphorylation signal observed for PIN2 HL S2,3A suggested that these two sites are the key phosphorylation targets for AGC3-4 (Fig. 8A,B), whereas PID was still able to produce a significant phosphorylation signal with this mutant protein (Fig 8C,D). This difference in phosphorylation specificity might be important for the effect of AGC3-4 on basal PIN polarity, since it was shown that phosphorylation of all three serines is necessary for full PIN1 and PIN2 functionality and apical polarity (Huang *et al.*, 2010). We hypothesize that *in vivo* AGC3-4 is able to phosphorylate PIN hydrophilic loops, however with slightly different substrate specificity compared to the other three AGC3 kinases, leading to partial phosphorylation of the three conserved serines and as a result to recycling of PINs to the basal plasma membrane.

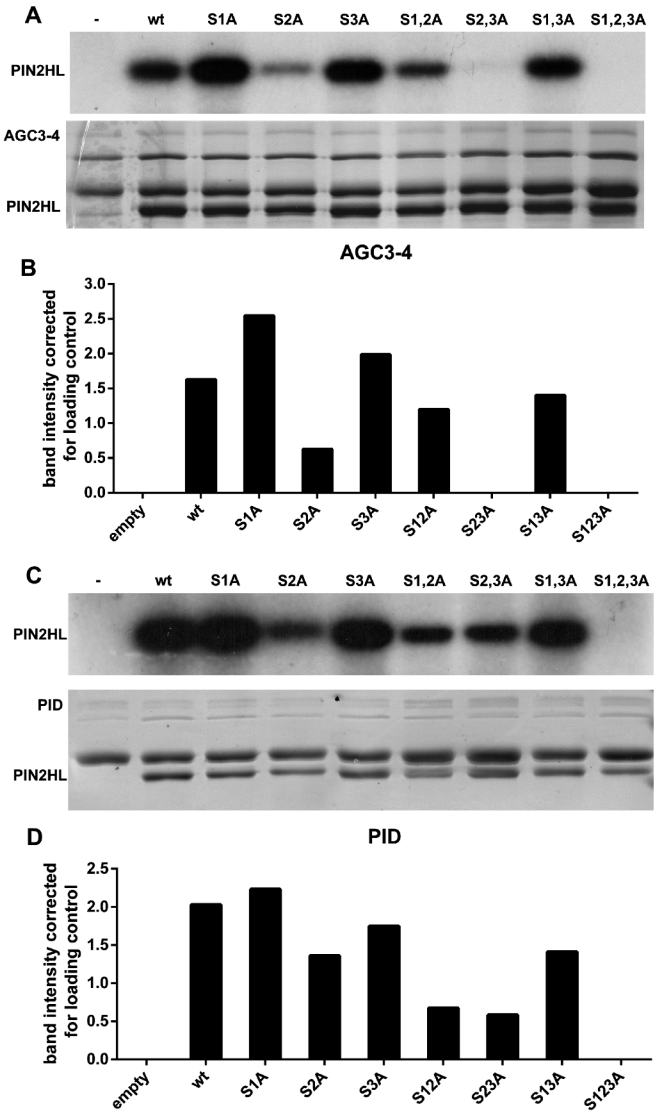

Figure 8: AGC3-4 and PID phosphorylate the TPRXS motifs in the PIN2 hydrophilic loop with different specificity.

(A-D) *In vitro* phosphorylation assay where the purified GST-tagged hydrophilic loop of PIN2 (PIN2 HL) and mutants in the three TPRXS motifs were tested for phosphorylation with purified GST-tagged AGC3-4 (A,B) or -PID (C,D). The upper image in (A,C) depicts the autoradiograph and the lower image the Coomassie stained gel used as loading control (lowest band used) PIN2. (B,D) Quantification of the band intensity (arbitrary units) of the respective autoradiographs of (A) and (C) relative to the loading control intensity, with the empty lane set at 0.

Discussion

The Arabidopsis AGC kinases PID, WAG1 and WAG2 are well established PIN polarity regulators that determine the asymmetric distribution of 'long' PIN proteins over the plasma membrane by phosphorylating specific serine residues in their large central hydrophilic loop. Based on sequence homology, they group in the AGC3 clade together with a fourth kinase AGC3-4 (Galván-Ampudia and Offringa, 2007; Rademacher and Offringa, 2012). A previous report suggested that AGC3-4 acts redundantly with the other three AGC3 kinases (Cheng et al., 2008), however, this was based on a suggested minimal contribution to the embryo phenotype. Here we studied the role of AGC3-4 in detail, and show that AGC3-4 acts opposite to the other AGC3 kinases, despite the fact that it phosphorylates the same serine residues in the TPRXS motifs in the PIN hydrophilic loop (this study, Dhonukshe et al., 2015; Huang et al., 2010).

AGC3-4 acts opposite to PID in promoting basal PIN1 and PIN2 polarity.

Although *AGC3-4* did not act redundantly to the other AGC3 kinases, there were some effects of single mutant *agc3-4* and *35S::AGC3-4* plants that hinted towards changes in auxin transport. Although *PID::AGC3-4* was not able to fully complement the *pid wag1 wag2* triple mutant, there was at least a partial complementation in rosette growth. Interestingly this was also the case when *PID::WAG2* was used to complement this triple mutant. *PID::AGC3-4* and *PID::WAG2* also had the similar effects on cotyledon development and were not able to fully complement the *pid wag wag2* mutant phenotype. However when the AGC3 kinases are overexpressed the phenotype of *35S::AGC3-4* is markedly different, also from that of *35S::WAG2* (Dhonukshe et al., 2010). Thus most obvious difference between AGC3-4 and the other three AGC3 kinases is the lack of PIN1 and PIN2 apicalization when *AGC3-4* is overexpressed. Instead, we found support for an increase in relative basal localization of PIN1 and PIN2 in respectively the stele and the cortex in the root meristem of *AGC3-4* overexpression seedlings. In the case of PIN1 the amount of lateral PIN1 decreased, leading to a relative abundance of basal PIN1. The observed increase in BFA bodies for PIN1 in the stele and for PIN2 in the epidermis of *35S::AGC3-4-CFP* root meristems further supports this notion, since increased basal targeting makes PINs more sensitive to BFA treatment (Kleine-Vehn et al., 2009). The changes in PIN localisation were also reflected in a subtle change in auxin distribution in the root tip, as indicated by the *35S::DII-YFP* reporter. The relatively reduced auxin levels in the root stele can be explained by an enhanced basal transport, however, if all PINs are more basal this should lead to elevated auxin levels in the root tip, something that is clearly not observed in the *AGC3-4* overexpression seedlings. Presumably, the effect of *AGC3-4* overexpression on PIN polarity in the outer layers of the root tip is complicated by the co-expression of the other *AGC3* kinase genes.

However, the fact that both *agc3-4* loss-of-function and *AGC3-4* overexpression lead to a decreased root gravitropic response might be explained by AGC3-4's proposed function of promoting basal PIN localization. *AGC3-4* is predominantly expressed in the (pro)vascular tissue throughout the plant (this study, Cheng et al., 2008), so if basal auxin transport in the (pro)vascular tissue, is slightly impaired by reduced basal PIN localisation in the *agc3-4* loss-of-function mutant background, this is likely to lead to reduced auxin in the root tip, and thus to a reduced root growth and gravitropic response (Geisler et al., 2014). On the other hand, *AGC3-4* overexpression was shown to affect PIN2 in the cortex and epidermis, where AGC3-4 is normally not or only weakly present, which might disrupt the tightly controlled dynamic PIN2 localisation in these cell layers that mediates the root gravitropic responses (Abas et al., 2006; Baster et al., 2012; Kleine-Vehn et al., 2008b; Sukumar et al., 2009).

The delayed lateral root emergence might be explained by an enhanced basal flow of auxin, which deprives the tissues surrounding the lateral root primordia of auxin, causing a delayed or impaired outgrowth (Péret et al., 2013). This is in line with the observation that the delay is overcome by exogenous auxin. The increased apical dominance in adult *35S::AGC3-4-CFP* plants is not easily be explained by an increase in basal PINs, since blocking polar auxin transport by NPA application leads to increased branching (Bennett et al., 2006).

AGC3-4 promotes basal polarity by partial phosphorylation of PINs.

In vitro kinase assays showed that AGC3-4 phosphorylates the same serine residues in the TPRXS motifs as PID, WAG1 and WAG2. This puts forward the question as to how AGC3-4 promotes basal PIN localisation, whereas the other three AGC kinases have the reverse effect. More careful analysis of the *in vitro* kinase assay revealed that AGC3-4 did not phosphorylate the serine in motif 1 (S1), implying that in tissues that predominantly express *AGC3-4* most PINs will be phosphorylated at S2 and S3, but not at S1. It is known by mutant analysis that PIN1 and PIN2 need to be fully phosphorylated at S1,2,3A to be able to complement *pin1* and *pin2* mutants respectively and that even single phosphorylation site mutants display altered polarity (Huang et al., 2010). Partial phosphorylation by AGC3-4 could thus lead to a different cycling of PIN1 and PIN2 to and from the plasma membrane and more concrete this partial phosphorylation could lead to an increase in uptake of PINs into GNOM-dependent vesicles, which are targeted basally (Fig. 9).

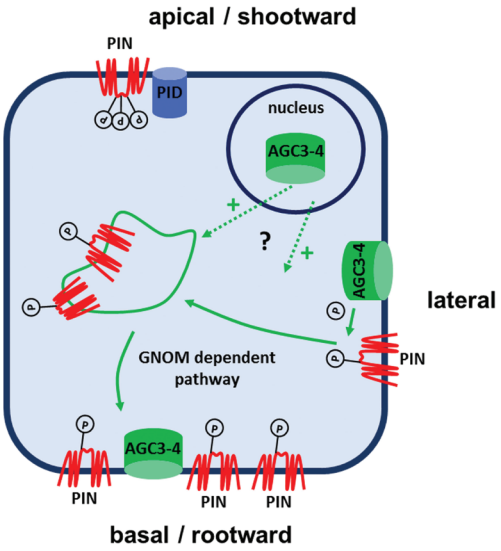

Figure 9: Model for the proposed role of AGC3-4 in regulating basal targeting of PIN1 and PIN2.
PINHL Phosphorylation by AGC3-4, which is partial compared to full phosphorylation by PID, results in PIN vesicles to be cycled through the GNOM dependent pathway to the basal side of the cell, instead of cycling to the apical side of the cell in the case of full PID-mediated phosphorylation. The role of AGC3-4 in the nucleus is not yet clear.

A nuclear role for AGC3-4

The subcellular localization of AGC3-4 may be an important differential trait compared to PID, since it was found to be weakly localized to the plasma membrane *in vivo* and much stronger in the nucleus. The function of this nuclear presence is yet unknown, but there are a few interesting possibilities.

PIN6 has an intermediate sized HL that still contains two TPRXS motifs, and its reported localization in the ER makes it tempting to speculate that AGC3-4 regulates the activity or localization of this PIN, either by inducing its localisation at the PM, or by controlling the rate of auxin transport from the ER into the nucleus (Bosco et al., 2012; Mravec et al., 2009; Sawchuk et al., 2013). The PIN6 HL however lacks the second TPRXS motif, which was shown to be most prominently phosphorylated by all AGC3 kinases (this study, Dhonukshe et al., 2015).

For the PID ortholog in maize BARREN INFLORESCENCE 2 (BIF2) it was shown that it can phosphorylate the transcription factor BARREN STALK 1, which is involved in inflorescence development (Skirpan et al., 2008ta). This suggests a potential function for AGC3-4 in regulating (nuclear) transcription factors, something that AGC kinases are known to do in animal cells (Uhle et al., 2003). The phenotypes that cannot be directly explained by the enhanced basal PIN localisation in AGC3-4 overexpression lines, such as the dwarf growth and strong apical dominance, might be a consequence of its function in the nucleus.

The localization in nuclear speckles, which was clearly observed in protoplasts, is similar to that of photobodies, which contain the phytochromes and a large collection of light-regulating factors (Van Buskirk et al., 2012). It would be interesting to investigate if AGC3-4 is in any way involved in photomorphogenesis or light regulation.

Possible overlapping functions with other AGC kinases.

To explain why *agc3-4* mutant plants have such a subtle phenotype we consider possible overlapping functions with the closely related D6 protein kinases (D6PKs), which are are part of the AGC1 kinase clade (Galván-Ampudia and Offringa, 2007). D6PK and the related D6PK-likes (D6PKL) can also phosphorylate the PIN1 and PIN2 hydrophilic loop, but with a different substrate specificity. It has been suggested that D6PK phosphorylation activates the transport capabilities of the PIN auxin efflux carrier, instead of changing its localization, and that together with PID it is necessary for plant development (Barbosa et al., 2014; Zourelidou et al., 2014). In support of this, the quadruple D6PK(L) mutant mimics the *pin-formed* phenotype (Willige et al., 2013; Zourelidou et al., 2009). The insertion domain between the kinase domains, containing the kinase activation segment, of AGC3-4 and D6PK are of similar length and different to that of PID (or WAG1/2) (Rademacher and Offringa, 2012). However the phosphorylation by D6PK on PIN1 and PIN2 does not take place at the same residues as used by the AGC3 kinases, and D6PK overexpression does also not result in the same basal-to-apical shift observed with PID overexpression (Dhonukshe et al., 2010; Zourelidou et al., 2014). The different residues preferred by D6PK and AGC3-4 make it unlikely that they function in the same fashion.

Besides the D6 kinases, other AGC kinases are either clearly different (*Phot1* and *Phot2*), not involved in polar auxin transport regulation (e.g. *OXI1, UCN*: Camehl et al., 2011; Enugutti et al., 2012) or are not yet well-studied (Rademacher and Offringa, 2012).

Another explanation may well be that any phenotypes of *agc3-4* might be masked by growing conditions. It is clear that *Arabidopsis* plants are growing quite different in growth chambers when compared to growth in the open field, in particular with regard to water, nutrient, temperature and light levels (Poorter et al., 2016).

Closing statement

Previously, the AGC3-4 kinase has been called PID2 based on high amino acid sequence similarity with PID (Cheng *et al.*, 2008). Our results show, however, that this name is not correct, as the two kinases have an opposing role in PIN polarity establishment, PID directing PINs to the apical side, and AGC3-4 promoting basal PIN localisation. Since AGC3-4 acts differently on PIN plasma membrane localization and has a different *in vitro* phosphorylation specificity compared to PID, it will be interesting to know how phosphorylation of the PIN hydrophilic loop translates into a polarity cue. It is likely that there are co-regulators of polarity that are themselves also polarly localized in the cell, which may help to translate phosphorylation of the PIN hydrophilic into the recruitment of endocytosis and exocytosis factors.

Materials and Methods

Plant material and growth conditions

For *agc3-4* loss-of-function mutants we used T-DNA insertion alleles *agc3-4-1* (SAIL269_G07, Cheng et al., 2007) and *agc3-4-2* (SAIL_1262_B11), see Fig. S3 for overview of the *AGC3-4* gene. The *pid-14* (SALK_049736), *wag1* (SALK_002056), *wag2* (SALK_070240), *pPIN2::PIN2-YFP (S1,2,3A), pid-14 PID::PID-YFP* and *WAG1::WAG1-GFP* lines were described previously (Dhonukshe *et al*., 2010). Construction of *PID* and *AGC3-4* overexpression and *AGC3-4* complementation lines is described below. For plate growth, *Arabidopsis* seeds were surface sterilized by a 30 seconds wash with 70% ethanol, followed by 10 minutes incubation in 50% commercial bleach solution (1% chlorine). Seeds were subsequently rinsed five times with sterile water. Seeds were vernalized for 5 days in dark at 4°C and germinated on ½ MS medium supplemented with 1% sucrose and 0.8% Daichin agar and antibiotics when required (21°C, 16 h-photoperiod, 70% humidity and a PAR of 70-90 µmol/m^2/s). For mature plant growth, seeds were sown onto soil after overnight vernalization on wet filter paper in the dark at 4°C, or they were transferred after two weeks of growth on ½ MS plates. Plants were grown at 21°C and 70% relative humidity with a 16 hr photoperiod (PAR 140 µmol/m2/s). All primers for genotyping can be found in table S1.

Molecular cloning

All oligonucleotides used for cloning procedures are described in table S1. The pGEX-PID (Benjamins *et al.*, 2003) and pGEX-PIN2HL (Abas *et al.,* 2006) constructs have been described previously. The mutant PIN2 HL constructs were made with the Quickchange XL site-directed mutagenesis kit (Stratagene) as described previously (Dhonukshe et al., 2010). For construction of the *PIDpro* driven *AGC3* constructs the pGreenII-based destination vector was used, where the Gateway recombination cassette was inserted in frame with the *YFP* coding region into pGreenII0179 and pGreenII0229. The coding regions of *PID, AGC3-4*, *WAG1* and *WAG2* were amplified from *Arabidopsis thaliana* ecotype Columbia (Col-0) cDNA from siliques using the Gateway cloning primers described in table S1 and cloned into pDONR207 using BP recombinase (Invitrogen). The promoter region of *PID* (3065bp upstream of the start codon) was amplified from *Arabidopsis thaliana* Col-0 genomic DNA using the primer set PID prom *Xho*I F - PID prom *Xho*I R and ligated into the pGEM-T Easy vector (Promega). From this plasmid the *PID* promoter fragment was excised as an *Xho*I fragment and cloned into the pGreenII0179YFP-HA destination vector. Expression vectors pGreenII0179 *PIDpro::PID-YFP-HA*, pGreenII0179 *PIDpro::WAG1-YFP-HA*, pGreenII0179 *PIDpro::WAG2-YFP-HA* and pGreenII0179 *PIDpro::AGC3-4-YFP-HA* were subsequently obtained by LR recombinase- mediated (Invitrogen) cloning of the appropriate coding region . For the pGEX-based destination vector, the Gateway recombination cassette was inserted in frame with the GST coding region. The construction of *pART7*-based CFP/YFP/

mRFP Gateway destination vectors was described previously (Dhonukshe *et al.*, 2010). Expression vectors pGEX-PID, pGEX-WAG1, pGEX-WAG2, pGEX-AGC3-4, pART7-PID-CFP, pART7-PID-mRFP, pART7-WAG1-mRFP, pART7-WAG2-mRFP, and pART7-AGC3-4-CFP/mRFP were constructed by LR recombinase-mediated cloning of the appropriate coding region into either the pGEX-based destination vector for N terminal fusions with the *Glutathione-S-transferase* (*GST*) coding region, or the pART7-based destination plasmids. Expression cassettes of pART7-AGC3-4-CFP/YFP and pART7-PID-mRFP were cloned into the pART27 binary vector by *Not*I digestion and ligation (Gleave, 1992). Bacteria were grown on LC medium supplemented with 100 µg/mL carbenicillin or 10 µg/mL gentamicin for *E. coli* strain DH5α containing pDONR207, pART7 or pGEX-based plasmids, or 50 µg/mL kanamycin (Km) for *E. coli* strain DH5α. Binary plasmids were introduced into *Agrobacterium tumefaciens* strain AGL1 by electroporation and selection on LC medium containing 20 µg/ml rifampicin and 50 µg/mL Km.

Plant transformation

Arabidopsis agc3-4 AGC3-4::AGC3-4-YFP plant lines were obtained by *Agrobacterium*-mediated transformation of the *agc3-4-1* allele by floral dipping (Davis et al., 2009) using *Agrobacterium* strain AGL1 containing the pGREENII0179 *pAGC3-4::AGC3-4-YFP*. T1 and T2 generations were selected on plates with timentin (only T1, 100mg/l) and hygromycin (20mg/l). T2 plants were screened for single locus T-DNA inserts, and homozygous transgenic lines were selected in the T3 generation using antibiotic resistance

Arabidopsis lines transgenic for *35S::PID-RFP* or *35S::AGC3-4-CFP* (*DII-YFP*) were obtained by the same floral dip transformation and subsequent selection, as described above, using *pART27:35S::PID-RFP* or *pART27:35S::AGC3-4-CFP* and Col-0 as the background genotype and 25mg/l kanamycin as the selection marker.

BFA Treatment

Four days old vertically grown seedlings were used for BFA treatments. We incubated around 20 seedlings in culture plates with liquid ½ MS medium with 1% sucrose and 25 µM BFA diluted in DMSO. Seedlings were kept in liquid medium containing BFA for 4 or 6 hours and treatments were synchronized so that seedlings were fixed for immunodetection at the same time.

PIN1 and PIN2 immunodetection

Immunodetection was performed on 4 days old seedlings grown vertically on solid ½ MS medium with 1% sucrose according and fixation and immunodetection was performed according to the protocol of Sauer et al., (2006). The antibodies used and their dilutions were 1:800 for goat anti-PIN1 (Agrisera), 1:1000 for rabbit anti-PIN2 (Agrisera), 1:600 for

donkey anti-Goat-Alexa Fluor ® 555 (Life Technologies), and 1:600 for donkey anti-Rabbit-Alexa Fluor ® 488 (Life Technologies). Microscopy was performed as described below.

Protein purification

Cultures of *E. coli* strain Rosetta (Novagen) containing constructs *pGEX-GST-PID, pGEX-GST-AGC3-4* or *pGEX-GST-PIN2* hydrophilic loop (PIN2 HL) were grown at 37ºC to OD_{600}=0.6 in LC medium supplemented with 100 µg/mL carbenicillin (Cb) and 34 µg/mL chloramphenicol. The cultures were then induced for 4 hrs with 1 mM IPTG at 30ºC, and bacteria were harvested by centrifugation and frozen at -20ºC. Bacterial pellets were resuspended in 2.5ml extraction buffer (EB: 1x PBS, 2 mM EDTA, 2 mM DTT) supplemented with 0.1% Tween-20 and 0.1 mM of the protease inhibitors phenylmethanesulfonyl fluoride, leupeptin and aprotinin (Sigma). After sonication for 2 min, Triton X-100 was added to a final concentration of 1% and the mixture was incubated for 5 min on ice, followed by centrifugation at 15,000 x g for 20 min at 4°C. Supernatants were added to 400 µl of pre-equilibrated 50% Glutathione Sepharose 4B beads (GE Amersham) and incubated for 1 hr. Beads were washed three times with 500 µl EB. Purified proteins were recovered with 100 µl elution buffer (10mM reduced glutathione, 50 mM Tris-HCl pH 8.0) and analyzed by SDS-PAGE, blotted on a PDVF membrane (Millipore, USA) and immunodetected using anti-GST (Molecular Probes) according to the manufacturer's instructions.

***In vitro* phosphorylation assay**

Approximately 1 µg of each purified GST-tagged protein (kinase and substrates) was added to a 20 µl kinase reaction mix, containing 1x kinase buffer (25 mM Tris-HCl pH 7.5, 1 mM DTT, 5 mM MgCl2) and 1x ATP solution (100 µM MgCl2, 100 µM ATP-Na2+, 1 µCi 32P-γ-ATP). The mix was incubated at 30ºC for 30 minutes, after which the reaction was stopped by the addition of 5 µL of 5x protein loading buffer (310 mM Tris-HCl pH 6.8, 10% SDS, 50% Glycerol, 750 mM β-Mercaptoethanol, 0.125% Bromophenol Blue). Reactions were subsequently separated over 10% polyacrylamide gels, which were washed three times for 30 minutes with kinase gel wash buffer (5% Trichloroacetic Acid, 1% Na2H2P2O7), Coomassie stained and dried. Autoradiography was performed for 24-48 hrs at -80ºC using Fuji Super RX X-ray films and intensifier screens.

Arabidopsis protoplast transfection

Protoplasts were obtained from *Arabidopsis* cell suspension cultures as described previously (Schirawski et al., 2000). Plasmid DNA was purified using a Qiagen Midi Kit. Per $2{,}5*10^5$ protoplasts, 7,5 µg of plasmid was used for transfection. After transfection protoplasts were incubated overnight in 4,5 ml culture medium B (Schirawski et al., 2000) in 6-well plates in the dark 24ºC, 70 % humidity.

Confocal microscopy and analysis

Four to seven day old seedlings were mounted in water on glass slides. Roots were imaged using an upright Zeiss LSM5 LCSM with a 458 (CFP)/ 488(GFP)/ 514(YFP)/ 543(mRFP) nm excitation laser and 475-525 nm, 505-530 nm, 530-600 nm, or 560-615 band pass emission filters for CFP, GFP, YFP, or RFP, respectively. Autofluorescence in Fig. 4E,F was also captured by placing LP650 filter in front of the detector. Root images were captured with a 40x 1.2NA water objective. Overnight-incubated protoplasts were pipetted into 8-well coverslips and imaged with an inverted Zeiss LSM5 microscope with an 63x 1.3NA oil objective using the same laser and band-pass filters described above.

The quantifications in figures 6,7 and 8 were performed with ICY (de Chaumont et al., 2012). All images of an analyzed set were captured using the same laser, pinhole and detector settings. DII-YFP intensities were determined by comparing the mean pixel intensities of the regions indicated in Fig. 6D of ten root tips per treatment. PIN1 and PIN2 ratio measurements were performed on 10 cells per image, and 5 to 10 images were used per treatment. Of each measured cell, the inner lateral side was measured that could be attributed to that particular cell with certainty. The amount of BFA bodies were measured manually by analyzing optical sections made from one cell layer of the epidermis (PIN2) and the endodermis + 1st layer of stele (PIN1) in the root tip. The amount of cells counted per seedling was on average 22 for PIN1 and 11 for PIN2. Statistical analysis was performed with Graphpad Prism software.

Phenotyping

Plants were grown under long day conditions described above. Rosette diameters and leaf areas were measured with Rosette Tracker (De Vylder et al., 2012) using images taken with a regular camera setup. Root, hypocotyl and gravitropism measurements were taken from seedlings grown on ½ MS agar plates with 1% sucrose and images were analyzed using ICY (de Chaumont et al., 2012). Gravitropism experiments were performed by transferring seedlings to a new plate to straighten the roots. Plates were then incubated vertically under normal growth conditions for one hour to acclimatize the seedlings, and were subsequently turned 90 degrees to start the geotropic growth experiment. Images were taken at the start and every 2 hours using a regular camera setup. The efficiency of auxin-induced lateral root formation was determined by germinating seedlings on ½ MS plates with 1% sucrose without hormones. After four days seedlings were transferred to plates containing 50 nM 1-NAA or 0.1 µM 2,4-D. Seedlings were cleared using the protocol of Malamy and Benfey, 1997, and images were taken using a DIC microscope Statistical analysis was performed with Graphpad Prism software.

Supplemental data

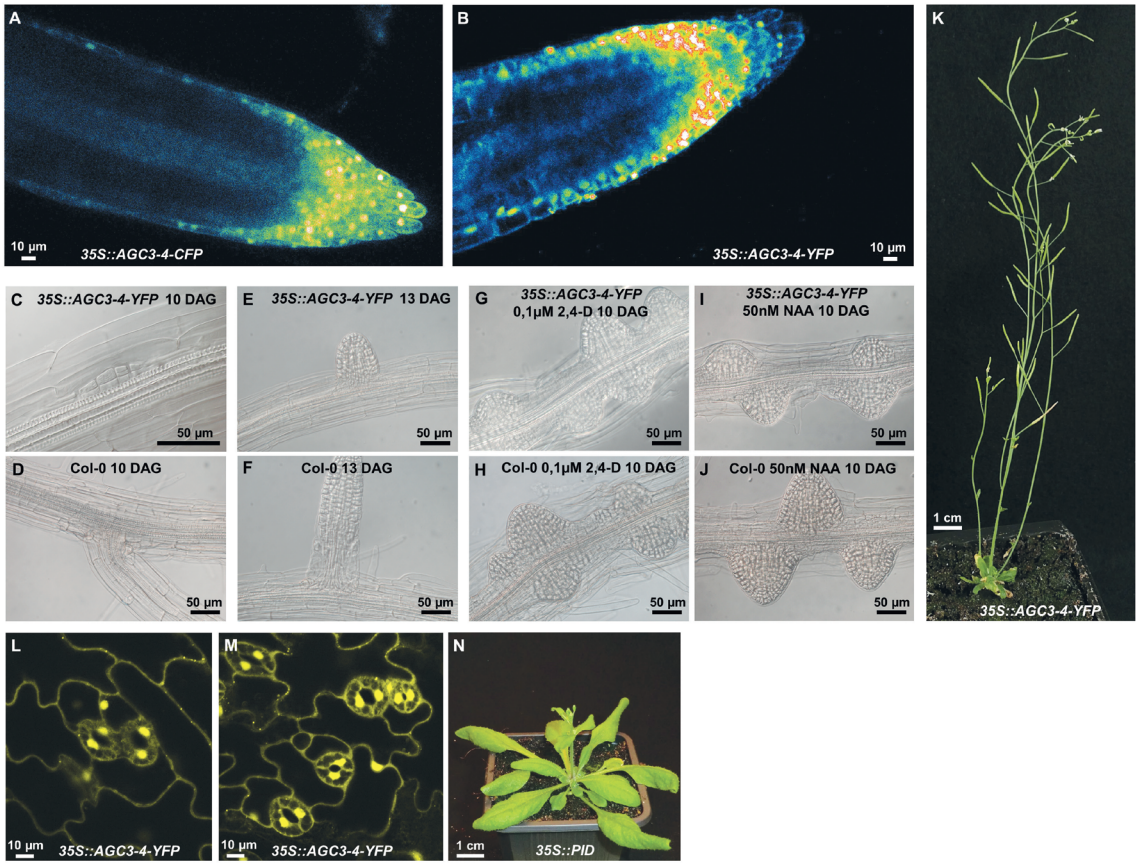

Figure S1: Various developmental phenotypes and confocal images of *35S::AGC3-4:CFP/YFP* seedlings. (A,B) *35S::AGC3-4-CFP/YFP* expression was verified using confocal microscopy of the root meristem of five day old seedlings. (C-F) Lateral root primordia and emerged lateral roots of wild type (Col-0) and *35S::AGC3-4-YFP* seedlings, ten or thirteen days after germination (DAG). (G-J) Response of wild type (Col-0) and *35S::AGC3-4-YFP* seedlings to 0,1µM 2,4-D or 0,05µM 1-NAA. Four day old seedlings were transferred to 1-NAA or 2,4-D containing medium and grown for four more days. (K) Two months old *35S::AGC3-4-YFP* plant. (L-M) AGC3-4-YFP overexpression in the leaf epidermis leads to occasional stomatal clustering. (N) Phenotype of one month old *35S::PID* plant.

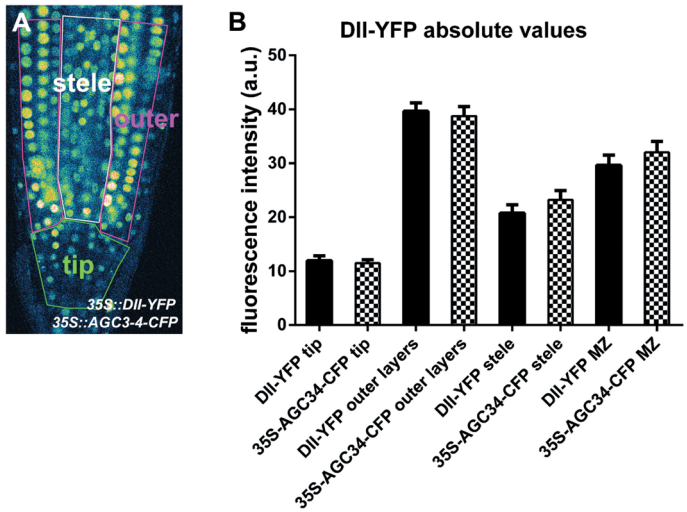

Figure S2: Quantification of DII-YFP intensity in root meristem regions.
(A) Tip =QC + columella stem cells; outer layers = epidermis + endodermis + cortex; stele = provascular tissue, meristem zone (MZ) = outer layers + stele. All confocal images used for quantification were taken using the same microscope settings. The error bars depict the standard error of the mean. No significant difference was observed between wild-type and *35S::AGC3-4-CFP* root meristems (two-way Anova). (B) DII-YFP mean fluorescence intensity per pixel (arbitrary units) in root meristems of four day old wild-type and *35S::AGC3-4-CFP* seedlings.

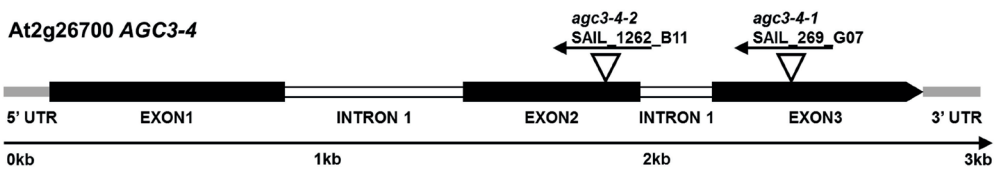

Figure S3: *AGC3-4* gene structure.
Gene structure of At2g26700 (*AGC3-4/PID2*), showing the localization and direction of T-DNA insertion alleles *agc3-4-1* (SAIL_269_G07) and *agc3-4-2* (SAIL_1262_B11), based on data from T-DNA express (http://signal.salk.edu/cgi-bin/tdnaexpress) and thalemine (https://apps.araport.org/thalemine).

Table S1

Primer name	Target gene	sequence	remarks
SAIL1262B11 LP 2	At2g26700	AATCACATGGACCTCAA	*agc3-4-2* genotyping
SAIL1262B11 RP 2	At2g26700	GCTTTCTTATCCACTACG	*agc3-4-2* genotyping
SAIL269G07 F	At2g26700	CTTCTTCTTGTTCTCGTGT	*agc3-4-1* genotyping
SAIL269G07 R2	At2g26700	ATGAAACGTCGAAAGC	*agc3-4-1* genotyping
LB1 (SAIL)	N/A	GCCTTTTCAGAAATGGATAAATAGCCTTGCTTCC	left border primer SAIL
pid-14 LP	At2g34650	CAGTCGGGAAACTCAACTGTC	*pid-14* genotyping
pid-14 RP	At2g34650	ATTTTGCGATGAAAGTTGTGG	*pid-14* genotyping
wag1-1 LP	At1g53700	TATATTGCGCAGGGTTTGTTC	*wag1* genotyping
wag1-1 RP	At1g53700	TCTCGATCTCAGCTTCACCTC	*wag1* genotyping
wag2-1 LP	At3g14370	TAAAGGAATATTCCGAACGCC	*wag2* genotyping
wag2-1 LP	At3g14370	CCAAAACCCCCAAACATAAAC	*wag* genotyping
lbb1.3 (SALK)	N/A	ATTTTGCCGATTTCGGAAC	left border primer SALK
PID attB F	At2g34650	GGGGACAAGTTTGTACAAAAAAGCAGGCTTCAGCAT GTTACGAGAATCAGACGGT	*PID* gateway cloning
PID attB R -stop	At2g34650	GGGGACCACTTTGTACAAGAAAGCTGGGTCAAAGTA ATCGAACGCCGCTGG	*PID* gateway cloning
AGC3-4 attB F	At2g26700	GGGGACAAGTTTGTACAAAAAAGCAGGCTTCAG CATGGCTAATTCTAGTATCTTT	*AGC3-4* gateway cloning
AGC3-4 attB R -stop	At2g26700	GGGGACCACTTTGTACAAGAAAGCTGGGTCAAAATA ATCAAAATAATTAGA	*AGC3-4* gateway cloning
WAG1 attB F	At1g53700	GGGGACAAGTTTGTACAAAAAAGCAGGCTTCAG CATGGAAGACGACGGTTATTAC	*WAG1* gateway cloning
WAG1 attB R -stop	At1g53700	GGGGACCACTTTGTACAAGAAAGCTGGGTC TAGCTTTTTACCCACATAATG	*WAG1* gateway cloning
WAG2 attB F	At3g14370	GGGGACAAGTTTGTACAAAAAAGCAGGCTTCAG CATGGAACAAGAAGATTTCTAT	*WAG2* gateway cloning
WAG2 attB R -stop	At3g14370	GGGGACCACTTTGTACAAGAAAGCTGGGTCAACGC GTTTGCGACTCGCGTA	*WAG2* gateway cloning
PID prom XhoI F	At2g34650	TACTCGAGCCGAACCAATTCTAGCAATA	*PID* promoter cloning
PID prom XhoI R	At2g34650	ATCTCGAGCGCCGGGAAAATCGAAGTTAAATCAAGA	*PID* promoter cloning
pDONR207 F	N/A	TCTTCCGACTGAGCCTTT	entry vector primer
pDONR207 R	N/A	AGCTGGATGGCAAATAATGA	entry vector primer
35S F	N/A	CGCACAATCCCACTATC	35S promoter primer
pART27 F	N/A	GAGCGGATAACAATTTCACACAG	Destination vector
PIN2HL S237A F	N/A	CATGATAACGCCGCGAGCTGCAAATCTCACC	PIN2HL mutagenesis
PIN2HL S237A R	N/A	GGTGAGATTTGCAGCTCGCGGCGTTATCATG	PIN2HL mutagenesis
PIN2HL S258A F	N/A	CCGACGCCGAGAGCTGCTAGCTTTAATCAG	PIN2HL mutagenesis
PIN2HL S258A R	N/A	CTGATTAAAGCTAGCAGCTCTCGGCGTCGG	PIN2HL mutagenesis
PIN2HL S310A F	N/A	CGTGACGCCGAGAACGGCAAATTTTGATGAGG	PIN2HL mutagenesis
PIN2HL S310A R	N/A	CCTCATCAAAATTTGCCGTTCTCGGCGTCACG	PIN2HL mutagenesis
PIN2HL S237E F	N/A	CATGATAACGCCGCGAGCTGAAAATCTCACCGG	PIN2HL mutagenesis
PIN2HL S237E R	N/A	CCGGTGAGATTTTCAGCTCGCGGCGTTATCATG	PIN2HL mutagenesis
PIN2HL S258E F	N/A	GCCGACGCCGAGAGCTGAGAGCTTTAATCAG	PIN2HL mutagenesis
PIN2HL S258E R	N/A	CTGATTAAAGCTCTCAGCTCTCGGCGTCGGC	PIN2HL mutagenesis
PIN2HL S310E F	N/A	GGCGTGACGCCGAGAACGGAAAATTTTGATGAGG	PIN2HL mutagenesis
PIN2HL S310E R	N/A	CCTCATCAAAATTTTCCGTTCTCGGCGTCACGCC	PIN2HL mutagenesis
pGEX-KG seq Fw	N/A	GGTATGGCTGTGCAGGTCGT	pGEX cloning primer

Acknowledgements

The authors would like to thank Paula van Kleef, Eike Rademacher and Adeline Rigal for help with the manuscript and Rene Benjamins and Ben Scheres for providing the *wag1 WAG1::WAG1-GFP line*. K.v.G. was supported by a NWO-CW TOP Grant (700.58.301) to R.O. from the Chemical Sciences Division with financial support from the Netherlands Organisation for Scientific Research (NWO).

References

Abas, L., Benjamins, R., Malenica, N., Paciorek, T., Wiśniewska, J., Wirniewska, J., Moulinier-Anzola, J. C., Sieberer, T., Friml, J. and Luschnig, C. (2006). Intracellular trafficking and proteolysis of the *Arabidopsis* auxin-efflux facilitator PIN2 are involved in root gravitropism. *Nat. Cell Biol.* **8**, 249–56.

Barbosa, I. C. R. C. R., Zourelidou, M., Willige, B. C. C., Weller, B. and Schwechheimer, C. (2014). D6 PROTEIN KINASE activates auxin transport-dependent growth and PIN-FORMED phosphorylation at the plasma membrane. *Dev. Cell* **29**, 674–85.

Baster, P., Robert, S., Kleine-Vehn, J., Vanneste, S., Kania, U., Grunewald, W., De Rybel, B., Beeckman, T. and Friml, J. (2012). SCF(TIR1/AFB)-auxin signalling regulates PIN vacuolar trafficking and auxin fluxes during root gravitropism. *EMBO J.* **32**, 260–274.

Benjamins, R., Quint, A., Weijers, D., Hooykaas, P. and Offringa, R. (2001). The PINOID protein kinase regulates organ development in *Arabidopsis* by enhancing polar auxin transport. *Development* **128**, 4057–67.

Bennett, T., Sieberer, T., Willett, B., Booker, J., Luschnig, C. and Leyser, O. (2006). The Arabidopsis MAX pathway controls shoot branching by regulating auxin transport. *Curr. Biol.* **16**, 553–563.

Bosco, C. D., Dovzhenko, A., Liu, X., Woerner, N., Rensch, T., Eismann, M., Eimer, S., Hegermann, J., Paponov, I. a, Ruperti, B., et al. (2012). The endoplasmic reticulum localized PIN8 is a pollen-specific auxin carrier involved in intracellular auxin homeostasis. *Plant J.* **72**, 860–870.

Brunoud, G., Wells, D. M., Oliva, M., Larrieu, A., Mirabet, V., Burrow, A. H., Beeckman, T., Kepinski, S., Traas, J., Bennett, M. J., et al. (2012). A novel sensor to map auxin response and distribution at high spatio-temporal resolution. *Nature* **482**, 103–106.

Camehl, I., Drzewiecki, C., Vadassery, J., Shahollari, B., Sherameti, I., Forzani, C., Munnik, T., Hirt, H. and Oelmüller, R. (2011). The OXI1 kinase pathway mediates Piriformospora indica-induced growth promotion in *Arabidopsis*. *PLoS Pathog.* **7**,.

Cheng, Y., Qin, G., Dai, X. and Zhao, Y. (2008). NPY genes and AGC kinases define two key steps in auxin-mediated organogenesis in *Arabidopsis*. *Proc. Natl. Acad. Sci. U. S. A.* **105**, 21017–22.

Davis, A. M., Hall, A., Millar, A. J., Darrah, C. and Davis, S. J. (2009). Protocol: Streamlined sub-protocols for floral-dip transformation and selection of transformants in *Arabidopsis thaliana*. *Plant Methods* **5**, 3.

de Chaumont, F., Dallongeville, S., Chenouard, N., Hervé, N., Pop, S., Provoost, T., Meas-Yedid, V., Pankajakshan, P., Lecomte, T., Le Montagner, Y., et al. (2012). Icy: an open bioimage informatics platform for extended reproducible research. *Nat. Methods* **9**, 690–696.

De Vylder, J., Vandenbussche, F., Hu, Y., Philips, W. and Van Der Straeten, D. (2012). Rosette tracker: an open source image analysis tool for automatic quantification of genotype effects. *Plant Physiol.* **160**, 1149–59.

Dhonukshe, P., Aniento, F., Hwang, I., Robinson, D. G., Mravec, J., Stierhof, Y.-D. and Friml, J. (2007). Clathrin-mediated constitutive endocytosis of PIN auxin efflux carriers in *Arabidopsis*. *Curr. Biol.* **17**, 520–7.

Dhonukshe, P., Huang, F., Galvan-Ampudia, C. S., Mähönen, A. P., Kleine-Vehn, J., Xu, J., Quint, A., Prasad, K., Friml, J., Scheres, B., et al. (2010). Plasma membrane-bound AGC3 kinases phosphorylate PIN auxin carriers at TPRXS(N/S) motifs to direct apical PIN recycling. *Development* **137**, 3245–55.

Ding, Z., Galván-Ampudia, C. S., Demarsy, E., Langowski, L., Kleine-Vehn, J., Fan, Y., Morita, M. T., Tasaka, M., Fankhauser, C., Offringa, R., et al. (2011). Light-mediated polarization of the PIN3 auxin transporter for the phototropic response in *Arabidopsis*. *Nat. Cell Biol.* **13**, 447–52.

Doyle, S. M., Haeger, A., Vain, T., Rigal, A., Viotti, C., Łangowska, M., Ma, Q., Friml, J., Raikhel, N. V, Hicks, G. R., et al. (2015). An early secretory pathway mediated by GNOM-LIKE 1 and GNOM is essential for basal polarity establishment in *Arabidopsis thaliana*. *Proc. Natl. Acad. Sci. U. S. A.* **112**, E806-15.

Enugutti, B., Kirchhelle, C., Oelschner, M., Torres Ruiz, R. A., Schliebner, I., Leister, D. and Schneitz, K. (2012). Regulation of planar growth by the *Arabidopsis* AGC protein kinase UNICORN. *Proc. Natl. Acad. Sci. U. S. A.* **109**, 15060–5.

Friml, J., Wiśniewska, J., Benková, E., Mendgen, K. and Palme, K. (2002). Lateral relocation of auxin efflux regulator PIN3 mediates tropism in *Arabidopsis*. *Nature* **415**, 806–9.

Friml, J., Yang, X., Michniewicz, M., Weijers, D., Quint, A., Tietz, O., Benjamins, R., Ouwerkerk, P. B. F., Ljung, K., Sandberg, G., et al. (2004). A PINOID-dependent binary switch in apical-basal PIN polar targeting directs auxin efflux. *Science* **306**, 862–5.

Furutani, M., Nakano, Y. and Tasaka, M. (2014). MAB4-induced auxin sink generates local auxin gradients in *Arabidopsis* organ formation. *Proc. Natl. Acad. Sci. U. S. A.* **111**, 1198–203.

Galván-Ampudia, C. S. and Offringa, R. (2007). Plant evolution: AGC kinases tell the auxin tale. *Trends Plant Sci.* **12**, 541–7.

Geisler, M., Wang, B. and Zhu, J. (2014). Auxin transport during root gravitropism: Transporters and techniques. *Plant Biol.* **16**, 50–57.

Geldner, N., Friml, J., Stierhof, Y.-D., Jurgens, G. and Palme, K. (2001). Auxin transport inhibitors block PIN1 cycling and vesicle traficking. *Nature* **413**, 425–428.

Geldner, N., Anders, N., Wolters, H., Keicher, J., Kornberger, W., Muller, P., Delbarre, A., Ueda, T., Nakano, A. and Jürgens, G. (2003). The *Arabidopsis* GNOM ARF-GEF mediates endosomal recycling, auxin transport, and auxin-dependent plant growth. *Cell* **112**, 219–30.

Gleave, A. P. (1992). A versatile binary vector system with a T-DNA organisational structure conducive to efficient integration of cloned DNA into the plant genome. *Plant Mol. Biol.* **38**, 455–1207.

Habets, M. E. J. and Offringa, R. (2014). PIN-driven polar auxin transport in plant developmental plasticity: A key target for environmental and endogenous signals. *New Phytol.* **203**, 362–377.

Huang, F., Kemel Zago, M., Abas, L., van Marion, A., Galván Ampudia, C. S. and Offringa, R. (2010). Phosphorylation of Conserved PIN Motifs Directs *Arabidopsis* PIN1 Polarity and Auxin Transport. *Plant Cell* **22**, 1129–1142.

Kleine-Vehn, J., Dhonukshe, P., Sauer, M., Brewer, P. B., Wiśniewska, J., Paciorek, T., Benková, E. and Friml, J. (2008a). ARF GEF-dependent transcytosis and polar delivery of PIN auxin carriers in *Arabidopsis*. *Curr. Biol.* **18**, 526–31.

Kleine-Vehn, J., Leitner, J., Zwiewka, M., Sauer, M., Abas, L., Luschnig, C. and Friml, J. (2008b). Differential degradation of PIN2 auxin efflux carrier by retromer-dependent vacuolar targeting. *Proc. Natl. Acad. Sci. U. S. A.* **105**, 17812–7.

Kleine-Vehn, J., Huang, F., Naramoto, S., Zhang, J., Michniewicz, M., Offringa, R. and Friml, J. (2009). PIN auxin efflux carrier polarity is regulated by PINOID kinase-mediated recruitment into GNOM-independent trafficking in *Arabidopsis*. *Plant Cell* **21**, 3839–49.

Kleine-Vehn, J., Wabnik, K., Martinière, A., Łangowski, Ł., Willig, K., Naramoto, S., Leitner, J., Tanaka, H., Jakobs, S., Robert, S., et al. (2011). Recycling, clustering, and endocytosis jointly maintain PIN auxin carrier polarity at the plasma membrane. *Mol. Syst. Biol.* **7**, 1–13.

Li, H., Lin, D., Dhonukshe, P., Nagawa, S., Chen, D., Friml, J., Scheres, B., Guo, H. and Yang, Z. (2011). Phosphorylation switch modulates the interdigitated pattern of PIN1 localization and cell expansion in *Arabidopsis* leaf epidermis. *Cell Res.* **21**, 970–978.

Malamy, J. E. and Benfey, P. N. (1997). Organization and cell differentiation in lateral roots of Arabidopsis thaliana. *Development* **124**, 33–44.

Mravec, J., Skůpa, P., Bailly, A., Hoyerová, K., Krecek, P., Bielach, A., Petrásek, J., Zhang, J., Gaykova, V., Stierhof, Y.-D., et al. (2009). Subcellular homeostasis of phytohormone auxin is mediated by the ER-localized PIN5 transporter. *Nature* **459**, 1136–40.

Péret, B., Middleton, A. M., French, A. P., Larrieu, A., Bishopp, A., Njo, M., Wells, D. M., Porco, S., Mellor, N., Band, L. R., et al. (2013). Sequential induction of auxin efflux and influx carriers regulates lateral root emergence. *Mol. Syst. Biol.* **9**, 699.

Petrásek, J., Mravec, J., Bouchard, R., Blakeslee, J. J., Abas, M., Seifertová, D., Wisniewska, J., Tadele, Z., Kubes, M., Covanová, M., et al. (2006). PIN proteins perform a rate-limiting function in cellular auxin efflux. *Science* **312**, 914–8.

Poorter, H., Fiorani, F., Pieruschka, R., Putten, W. H. Van Der, Kleyer, M. and Schurr, U. (2016). Tansley review Pampered inside , pestered outside ? Differences and similarities between plants growing in controlled conditions and in the field. *New Phytol.* 838–855.

Preuten, T., Hohm, T., Bergmann, S. and Fankhauser, C. (2013). Defining the site of light perception and initiation of phototropism in *Arabidopsis*. *Curr. Biol.* **23**, 1934–8.

Rademacher, E. H. and Offringa, R. (2012). Evolutionary Adaptations of Plant AGC Kinases: From Light Signaling to Cell Polarity Regulation. *Front. Plant Sci.* **3**, 250.

Santner, A. a and Watson, J. C. (2006). The WAG1 and WAG2 protein kinases negatively regulate root waving in *Arabidopsis*. *Plant J.* **45**, 752–64.

Sauer, M., Paciorek, T., Benková, E. and Friml, J. (2006). Immunocytochemical techniques for whole-mount in situ protein localization in plants. *Nat. Protoc.* **1**, 98–103.

Sawchuk, M. G., Edgar, A. and Scarpella, E. (2013). Patterning of leaf vein networks by convergent auxin transport pathways. *PLoS Genet.* **9**, e1003294.

Schirawski, J., Planchais, S. and Haenni, A. L. (2000). An improved protocol for the preparation of protoplasts from an established Arabidopsis thaliana cell suspension culture and infection with RNA of turnip yellow mosaic tymovirus: a simple and reliable method. *J. Virol. Methods* **86**, 85–94.

Sieburth, L. E., Muday, G. K., King, E. J., Benton, G., Kim, S., Metcalf, K. E., Meyers, L., Seamen, E. and Norman, J. M. Van (2006). SCARFACE Encodes an ARF-GAP That Is Required for Normal Auxin Efflux and Vein Patterning in *Arabidopsis*. *Plant Cell* **18**, 1396–1411.

Skirpan, A., Wu, X. and McSteen, P. (2008). Genetic and physical interaction suggest that BARREN STALK 1 is a target of BARREN INFLORESCENCE2 in maize inflorescence development. *Plant J.* **55**, 787–97.

Sukumar, P., Edwards, K. S., Rahman, A., Delong, A. and Muday, G. K. (2009). PINOID kinase regulates root gravitropism through modulation of PIN2-dependent basipetal auxin transport in *Arabidopsis*. *Plant Physiol.* **150**, 722–35.

Uhle, S., Medalia, O., Waldron, R., Dumdey, R., Henklein, P., Bech-Otschir, D., Huang, X., Berse, M., Sperling, J., Schade, R., et al. (2003). Protein kinase CK2 and protein kinase D are associated with the COP9 signalosome. *EMBO J.* **22**, 1302–12.

Van Buskirk, E. K., Decker, P. V. and Chen, M. (2012). Photobodies in Light Signaling. *Plant Physiol.* **158**, 52–60.

Willige, B. C., Ahlers, S., Zourelidou, M., Barbosa, I. C. R., Demarsy, E., Trevisan, M., Davis, P. a, Roelfsema, M. R. G., Hangarter, R., Fankhauser, C., et al. (2013). D6PK AGCVIII Kinases Are Required for Auxin Transport and Phototropic Hypocotyl Bending in *Arabidopsis*. *Plant Cell* **25**, 1674–1688.

Wisniewska, J., Xu, J., Seifertova, D., Brewer, P. B., Ru, K., Scheres, B., Blilou, I., Rouquie, D., Benková, E. and Friml, J. (2006). Polar PIN localization directs duxin flow in plants. *Science (80-.).* **312**, 833.

Xu, T., Wen, M., Nagawa, S., Fu, Y., Chen, J.-G., Wu, M.-J., Perrot-Rechenmann, C., Friml, J., Jones, A. M. and Yang, Z. (2010). Cell surface- and rho GTPase-based auxin signaling controls cellular interdigitation in *Arabidopsis*. *Cell* **143**, 99–110.

Zhang, K.-X., Xu, H.-H., Yuan, T.-T., Zhang, L. and Lu, Y.-T. (2013). Blue-light-induced PIN3 polarization for root negative phototropic response in *Arabidopsis*. *Plant J.* **76**, 308–321.

Zourelidou, M., Müller, I., Willige, B. C., Nill, C., Jikumaru, Y., Li, H. and Schwechheimer, C. (2009). The polarly localized D6 PROTEIN KINASE is required for efficient auxin transport in *Arabidopsis thaliana*. *Development* **136**, 627–36.

Zourelidou, M., Absmanner, B., Weller, B., Barbosa, I. C. R., Willige, B. C., Fastner, A., Streit, V., Port, S. a, Colcombet, J., de la Fuente van Bentem, S., et al. (2014). Auxin efflux by PIN-FORMED proteins is activated by two different protein kinases, D6 PROTEIN KINASE and PINOID. *e-life* **3**, 1–25.